Modeling Land–Atmosphere Interactions over Semiarid Plains in Morocco: In-Depth Assessment of GCM Stretched-Grid Simulations Using In Situ Data

Khadija Arjdal, Étienne Vignon, Fatima Driouech, Frédérique Chéruy, Salah Er-Raki, Adriana Sima, Abdelghani Chehbouni, Philippe Drobinski

Modeling land-atmosphere interactions over semi-arid plains in Morocco: in-depth assessment of GCM stretched-grid simulations using in situ data

Khadija Arjdal[*a,b], Étienne Vignon[b], Fatima Driouech[a], Frédérique Chéruy[b], Salah Er-Raki[c,d], Adriana Sima[b], Abdelghani Chehbouni[a], Philippe Drobinski[b]

[a]*Mohammed VI Polytechnic University, CSAES-International Water Research Institute (IWRI), Benguerir, Morocco*

[b]*Laboratoire de Météorologie Dynamique-IPSL, Sorbonne Université / CNRS / École Normale Supérieure-PSL Université / École Polytechnique-Institut Polytechnique de Paris, Paris, France*

[c]*Mohammed VI Polytechnic University (UM6P), CSAES-Center for Remote Sensing Applications (CRSA), Benguerir, Morocco*

[d]*ProcEDE/AgroBiotech center, Département de Physique Appliquée, Faculté des Sciences et Techniques, Université Cadi Ayyad, Marrakech, Morocco*

*Corresponding author: Khadija Arjdal. khadija.Arjdal@um6p.ma

Abstract:

Land surface-atmosphere interactions are a key component of climate modeling. They are particularly critical to understand and anticipate the climate and the water resources over the semi-arid and arid North-African regions. This study uses *in situ* observations to assess the ability of the IPSL-CM global climate model to simulate the land-atmosphere interactions over Moroccan semi-arid plains. A specific configuration with a grid refinement over the Haouz plain, near Marrakech, and nudging outside Morocco has been performed to properly assess the model's performances. To ensure reliable model-observation comparisons despite the fact that stations measurements are not representative of a mesh-size area, we carried out experiments with adapted vegetation properties. Results show that the CMIP6 version of the model's physics represents the near surface climate over the Haouz plain reasonably well. Nonetheless, the simulation exhibits a nocturnal warm bias, and the wind speed is overestimated in tree-covered meshes and underestimated in the wheat-covered region. Further sensitivity experiments reveal that LAI-dependent parameterization of roughness length leads to a strong surface wind drag and to underestimated land-surface atmosphere thermal coupling. Setting the roughness heights to the observed values improves the wind speed and to a lesser extent the nocturnal temperature. A low-bias in latent heat flux and soil moisture coinciding with a pronounced diurnal warm bias at the surface is still present in our simulations. Including a first-order irrigation parametrization yields more realistic simulated evapotranspiration flux and daytime skin surface temperatures. This result raises the importance of accounting for the irrigation process in present and future climate simulations over Moroccan agricultural areas.

Keywords:

General Circulation Model; Land-atmosphere interactions; Evaluation with in-situ data; Morocco

1. Introduction

The Mediterranean basin is one of the most vulnerable climate change hotspots (Diffenbaugh & Giorgi, 2012; Douville et al., 2021; Ali et al., 2022). Several parts of the region have registered a decrease in rainfall since 1960 with significant changes in the aridity and drought (Douville et al., 2021; Gutiérrez et al., 2021; Driouech et al., 2020). Soil moisture observations show that the Mediterranean region's aridity has been strongly influenced by rising temperatures and increased atmospheric demand (Vicente-Serrano et al., 2014; Gutiérrez et al., 2021). Furthermore, the sixth Assessment Report (AR6) and first MedECC Assessment Report (MAR1) show that climate models agree on a future warming ranging from 3.5°C to 8.75°C over the Mediterranean under the high-end scenario by the end of the 21st century (Cherif et al., 2020; Douville et al., 2021; Arjdal et al., 2023; Balhane et al., 2021). Climate change is projected to intensify throughout the region generating several cascading impacts on socio-economic sectors, including agriculture (Vafeidis et al., 2020).

Among the Mediterranean and North African countries, Morocco is considered as one of the most vulnerable countries to climate change (Schilling et al., 2020). Moroccan rainy season extends from October to April with a strong interannual precipitation variability (Born et al., 2010; Driouech, 2010). During the second half of the 20th century, the country experienced several below-average rainfall periods, mostly in winter and spring (Schilling et al., 2012; Fink et al., 2010; Meddi et al., 2010; Raymond et al., 2016, 2018a, 2018b) and is expected to experience more winter and spring dry spells in the future (Raymond et al., 2019). The observed trend towards a drier and warmer climate strengthens in future scenarios (Born et al., 2008; Driouech et al., 2020; Drobinski et al., 2020). A rising temperature by +1.4°C to +2.6°C is projected, while precipitation is projected to decrease by about 10% to more than 30% by 2065 (Marchane et al., 2017; Schilling et al., 2012; Tramblay et al., 2013; Arjdal et al., 2023).

The Moroccan economy, as most African countries, is heavily sustained by rainfed agriculture. This later contributes to about 13.6 % of the Global National Product (GNP) with 59% of agricultural areas used for cereal crops (Harbouze et al., 2019). During periodic droughts, groundwater remains the sole water resource. Combined effects of drought and water use, in particular owing to the spreading of urban and industrial regions, and an intensification of the use of irrigation for agriculture, led to a significant groundwater shortage in areas such as the Haouz Plain (31°30'0" N; 8°0'0" W), (Ait El Mekki and Laftouhi, 2016; Chehbouni et al., 2008). In fact, irrigated agriculture accounts for 85% of the total water use in the Haouz plain (Chehbouni et al., 2008), the Tensift watershed extending from the High Atlas Mountains being the major water source (Zkhiri et al., 2019).

Developing climate change adaptation strategies requires fine and accurate projections of the future climate which themselves rely on appropriate parameterization of the physical processes that govern the hydrological cycle and surface climate in climate models. In particular, the physical parameterizations of boundary layer processes and surface-atmosphere interactions play a fundamental role for the climate models performance and for determining their reliability to simulate and predict the surface climate (Betts, 2007; Cheruy et al., 2013; Santanello et al., 2018). Several studies evaluating climate models in the Mediterranean region have been carried out (e.g. Cavicchia et al., 2018; Drobinski et al., 2018; Panthou et al., 2018). However, most of the evaluations conducted rely on gridded datasets such as E-OBS, which has only a limited sub-dataset over Morocco, as highlighted in Cornes et al. (2018). Arjdal et al. (2023) evidenced large inter-model spread in projected surface hydrology over the North-African region by climate models involved in the latest CMIP exercise (CMIP6). This spread can be attributed either to differences in large scale circulation patterns or to discrepancies and uncertainties in simulating the parameterized atmospheric processes, the surface-atmosphere interactions as well as their responses to anthropogenic forcings. Regarding more specifically the Moroccan region, previous studies have assessed the dynamics and the variability of precipitation and characterized the water cycle (e.g., Driouech, 2010; Driouech et al., 2009; Tramblay et al., 2012, 2013). However, the ability of models to properly simulate the surface-atmosphere interactions remains under-explored. The main objective of this study is to perform a thorough evaluation of LMDZ-ORCHIDEE, the atmosphere-land surface component of IPSL-CM (The Institut de Pierre Simon Laplace Coupled Model, Boucher et al., 2020) in representing the land-surface atmosphere interactions in semi-arid conditions using rare and precious meteorological observations that were acquired over the Haouz Plain in Morocco. The IPSL-CM model has been historically and is still actively involved in the Coupled Model Intercomparison Projects (CMIP). A particular attention to the land surface-atmosphere coupling has been paid during the development of the successive versions (e. g., Aït-Mesbah et al., 2015; Cheruy et al., 2017, 2020; Hourdin et al., 2013; Wang et al., 2018) but never with a specific focus on the North-African or Mediterranean regions. We propose an approach to perform reliable model-observation comparisons and conclusive evaluation of the model's physics, leveraging the "zoom" capability of LMDZ to refine the grid over the plain and applying a nudging towards atmospheric reanalysis outside of the zoom area.

This manuscript is organized as follows: Sect. 2 presents the geographical setting, the observational datasets, the model simulations and the evaluation methodology. Results are presented and discussed in Sect. 3. Sect. 4 closes the paper with conclusions.

2. Data, model and methods:

a. Geographical setting and in situ measurements

The Haouz plain is located 40 km east of Marrakech city (central Morocco) and spreads over 20 450 km^2 (Khabba et al., 2013). It is delimited by the High-Atlas mountain to the south which represents the region's 'water tower' (Chehbouni et al., 2008) and the northern hills or jbilets, that is mountains with moderate relief that consists of rocky plains and hills located about 8 km north of Marrakech to the North (see Fig. 1). The climate of the region is semi-arid with annual average rainfall ranges to ~250 mm, primarily concentrated from autumn to spring. Average annual reference evapotranspiration (ETo) is of about 1600 mm (Er-Raki et al., 2010; Kharrou et al., 2011). Consequently, in order to maintain growth and productivity, constant irrigation is required in the fields (Chehbouni et al., 2008; Khabba et al., 2013). Major cultivation types include olives (40% of national production), oranges and wheat (Chehbouni et al., 2008; Khabba et al., 2013).

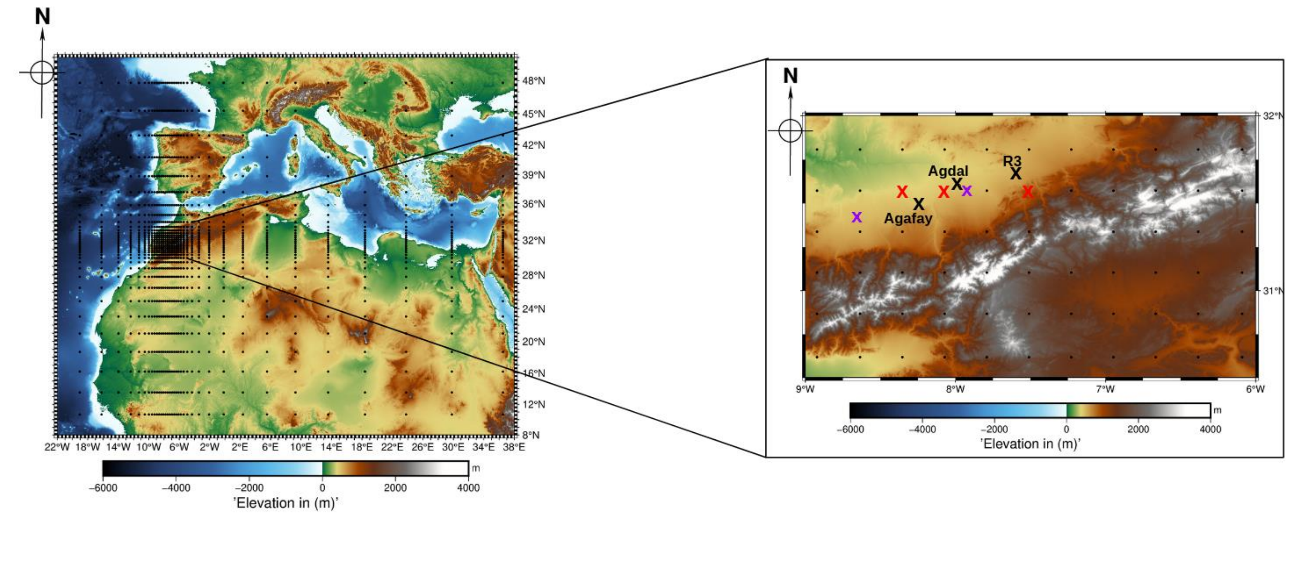

Figure 1 Map of the topography with a focus on the Haouz plain and the Atlas mountain range (inset). The black dots indicate the center of the model meshes. Black crosses show the location of the three main stations considered in this study, their corresponding model meshes are marked with red crosses. The location of the two additional stations Chichaoua and Graoua is indicated with purple crosses.

From the beginning of the 21th century, the Tensift watershed has been equipped with a network of meteorological and hydrological stations within the framework of the SUDMED Program, the measurement network has been managed by the Joint International Laboratory (LMI-TREMA) since 2011. Amongst the network (Figs. 2, S1), three stations are equipped with eddy-covariance systems, radiometers and soil heat flux measurements allowing for a detailed characterization of the energy and water exchanges between the land surface and the atmosphere. Those three stations, namely Agdal, Agafay and R3, will be used to evaluate the model. Two additional standard meteorological stations Graoua and Chichaoua respectively deployed in wheat fields - and for which we have access to long and high-quality time series - have been used. Their data help us assess whether the model performance - in terms of near surface wind, humidity and temperature - at the three main sites is comparable at two other sites in the plain (see details in Sect. B. of the Supplement).

Agafay site is located in an orange crop (38 ha), Agdal in an olive crop (275 ha) and R3 in a wheat crop field (2800 ha). The average height of trees is about 3 m in Agafay (Nassah et al., 2018) and 6 m in Agdal (Ezzahar et al., 2007). The R3 vegetation height can reach up to 0.74 m during the growing season. Meteorological measurements specifications are detailed in Table 1.

Measurements were sampled at either 1 or 20 Hz (see details in Table 1) and stored at 30 min intervals (Ezzahar et al., 2007). In the present study, 1-hour data averages are used in comparisons with model outputs. For each station, the selection of the time period considered to evaluate the model has been made by targeting the longest continuous time period for which the observational dataset has been consistent and thoroughly quality-checked. Thus, the periods (10/2002 - 11/2004), (01/2003 - 05/2003) and (09/2006 - 12/2009) have been considered respectively for Agdal, R3 and Agafay.

Quantity	**Instrument**	**Height from vegetation top**
Air temperature (T) Relative humidity (RH)	Vaisala HMP45AC probe	2 m
Wind direction Wind speed (U)	Young Wp200 anemometer	3.25 m (Agdal) 2 m (Agafay) 1.3 m (R3)
Precipitation	TRP525M Rain gauge	1 m
Downward shortwave radiation (SWdn) Upward shortwave radiation (SWup) Downward longwave radiation (LWdn) Upward longwave radiation (LWup) Surface temperature (Ts)	CNR1 radiometer	2 m
Sensible heat flux (H) Latent heat flux (Le) Friction velocity (u*)	20Hz three dimensional sonic thermo-anemometer (CSAT3) and open-path infrared gas analyzer (Li7500, LicorInc)	3.25 m (Agdal) 5.5 m (Agafay) 1.3 m (R3)
Soil moisture	CS616 water content reflectometer	5 cm depth

Table 1 Characteristics of the in situ measurements

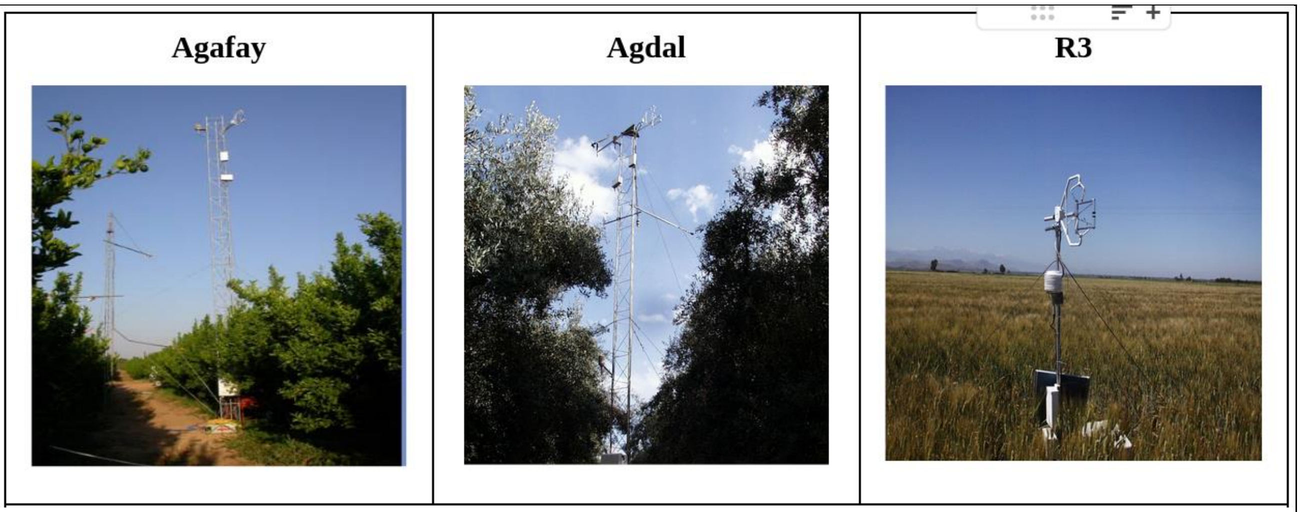

Figure 2 From left to right : Agafay, Agdal and R3 monitoring stations (Copyright : LMI-TREMA)

b. Model presentation, boundary layer and surface layer parameterizations

LMDZ is an atmospheric General Circulation Model (GCM) developed since the 80s (Sadourny and Laval, 1984) at Laboratoire de Météorologie Dynamique (LMD) and the atmospheric component of IPSL-CM. The ‘‘Z’’ in ‘‘LMDZ’’ refers to the zooming capability of its grid. LMDZ was intensively evaluated and developed for the tropical and equatorial regions (e.g., Diallo et al., 2017; Hourdin et al., 2015; Hourdin et al., 2020). Surface turbulent fluxes parameterization follows the Monin-Obukhov (MO) similarity theory and the details of the surface-layer scheme are given in Cheruy et al. (2020) and Vignon et al. (2017). The vertical turbulent diffusion follows a hybrid approach. First, the local mixing is parameterized using a TKE-l scheme based on the pioneering work of Yamada (1983) and revisited in Vignon et al. (2017). Second, the non-local mixing in the convective boundary layer is parameterized with a mass-flux scheme so-called the ‘thermal plume model’ (Hourdin et al., 2002, 2019; Jam et al., 2013; Rio et al., 2010).

In LMDZ, the sensible (H) and latent heat (Le) fluxes are calculated using a bulk formula between the surface and the first model level as follows:

$$H = \rho c_p C_h U_1 (\theta_{v1} - \theta_s) \quad (1)$$

$$L = \rho_1 \beta L_{vap} C_h U_1 \left(q_{v1} - q_{s,sat}\right) \quad (2)$$

with c_p is the specific heat of air at constant pressure, β is the aridity coefficient, $L_{vap}$is the latent heat of vaporization. ρ_1, U_1, θ_{v1} and $q_{v1}$are the air density, the wind speed, the virtual potential temperature and the specific humidity at the first model level respectively; θ_s and $q_{s,sat}$are the virtual potential temperature and the saturation specific humidity at the surface; C_h is the drag coefficient for heat, and reads:

$$C_h = \frac{\kappa^2}{\ln\left(\frac{z_1}{z_{0m}}\right)\ln\left(\frac{z_1}{z_{0h}}\right)} \times f_h \qquad (3)$$

Where z_1 is the first model level height, z_{0m} and z_{0h} are the roughness length for momentum and height respectively, and f_h is the stability function of the bulk Richardson number Ri_b between the first model level and the surface (Vignon et al., 2017).

The surface energy balance reads $R_n + H + Le + G = 0$ with H is the turbulent sensible heat flux, Le is the turbulent latent heat flux, G is the ground heat flux and R_n is the net radiative flux expressed as:

$$R_n = SW_{dn} - SW_{up} + LW_{dn} - LW_{up} \quad (4)$$

Where SW_{dn} is the downward shortwave radiation, SW_{up} is the upward shortwave radiation, LW_{dn} is the downward longwave radiation and LW_{up} is the upward longwave radiation. All fluxes are defined as positive towards the surface.

In climate simulations, LMDZ is coupled to the land surface model ORCHIDEE (Organising Carbon and Hydrology In Dynamic EcosystEms; Cheruy et al., 2020). ORCHIDEE consists in two sub-modules: i) SECHIBA (Schématisation des Échanges Hydriques à l'Interface Biosphère Atmosphère; Ducoudré et al., 1993) that computes the energy and the hydrological budgets, ii) STOMATE (Saclay Toulouse Orsay Model for the Analysis of Terrestrial Ecosystems; Botta et al., 2000) for phenology and carbon cycle. ORCHIDEE computes the exchanges between the soil and plant reservoirs. It provides to LMDZ the surface parameters needed to compute the energy and momentum fluxes at the interface with the atmosphere among which the roughness heights - which control the turbulent transfer of momentum (z_{0m}), heat and humidity (z_{0h}) between the surface and the atmosphere - the albedo and the aridity coefficient β. When coupled to LMDZ, the roughness heights in ORCHIDEE are by default computed as a function of the leaf area index (LAI) for each Plant Functional Type (PFT), using the model proposed by Massman (1999) and tested by Su et al. (2001). The thermal roughness length ($z_{0h)}$ is derived from z_{0m} as follows:

$$z_{0h} = \frac{z_{0m}}{\exp\ (\kappa B^{-1})} \qquad (5)$$

Where B^{-1} is the inverse Stanton number of heat transfer (Su et al., 2001) and κ = 0.41 is the Von Kármán constant. z_{0m} is usually higher than z_{0h} due to the fact that heat and humidity transfer are dominated by molecular diffusion, while the momentum transfer is mostly controlled by pressure forces (Garratt & Hicks, 1973; Su et al., 2001).

c. Configuration of the simulations and introduction of a bulk parameterization of irrigation.

In our simulations, we ran LMDZ with the 79-level vertical discretization used for CMIP6 and with a 64x64 horizontal grid centered on the Haouz plain (7.58 °W, 31.66 °N). The resolution at the center of the domain reaches 25 km x 25 km (Fig. 1). We apply nudging towards ERA5 reanalysis on the temperature, humidity and wind fields (as in Coindreau et al., 2007; Diallo et al., 2017 and Vignon et al., 2018) as follows:

$$\frac{\partial x}{\partial t} = F(x) - \frac{X - X^a}{\tau} \qquad (6)$$

Where X is either the temperature T, the specific humidity Q, the zonal and meridional wind U,V. F(x) is the operator describing the dynamical and physical processes that determine the evolution of X. X^a is the equivalent field from ERA5 and τ is the relaxation time that controls the nudging intensity (Coindreau et al., 2007; Vignon et al., 2018). We make the relaxation time vary from a small value ($\tau_{min} = 6h$) outside the zoom to a large value ($\tau_{max} = 240h$) inside the zoom such that the simulated fields over the Haouz plain are fully governed by the model physics and dynamics. We use the exact same physics configuration as the one developed and calibrated for the CMIP6 exercise, i.e. the so-called 6A version (Cheruy et al., 2020; Hourdin et al., 2020).

Simulations are performed for the period of available in-situ data (2000–2009). The first 2 years - which correspond to the spin- up time - are not included in the analysis. The vegetation in the land surface model ORCHIDEE is categorized into 15 Plant Functional Types (PFTs), including bare soil, which share similar structural properties (Lurton et al., 2020). PFTs are classified into eight forest classes, six grass/crop classes and the bare soil, with a varying partitioning at each grid cell. The default partitioning of land cover in grid cells corresponding to each of the studied stations is shown in Fig. 3. It is worth noting that the Agdal and Agafay weather stations are set-up in olive and orange orchards whose surface area is smaller than our 25 km x 25 km grid mesh size. Therefore, we carefully designed a methodology enabling the model-observations comparison despite the fact that the sites are not representative of the full corresponding grid mesh. Hence two simulation setups are considered: (i) the first one with the model's standard physics and land use map (STD); (ii) the second one with updated land use (CTRL) in which we set a unique PFT in each of the three grid cells corresponding to the 3 stations, the chosen PFT corresponding to the type of cultivation at the station (i.e Temperate Evergreen Broadleaf forests for Agdal and Agafay, and C3 crops for R3).

Note that in CTRL simulation, we only modify the vegetation cover in the mesh, not the soil texture, although soil properties also modulate the intensity of heat and water flux in the ground. In ORCHIDEE, the soil properties are taken from the prevailing soil texture (inferred from the Zobler (1986) map) within each mesh. At Agafay and Agdal, in situ observations show that the dominant soil texture is the “sandy class’, which is consistent with the soil properties prescribed in ORCHIDEE for the corresponding meshes. At R3 close to the Atlas foothills, a dominant clay fraction is observed (Er-Raki et al., 2007) which contrasts with the prevailing ‘sand’ category seen by ORCHIDEE. We have therefore run an additional simulation (CTRL-Txt, see Figs. S11, S12, S13 in the supplement) in which we have changed both the vegetation cover (as in CTRL) and the soil texture (prescribing a prevailing clay texture at the R3 model grid point). This simulation is presented in the supplementary materials but the key message here is that the differences between CTRL and CTRL-Txt at R3 in terms of near surface climate are very weak and that all the main conclusions drawn from the CTRL simulations also hold from CTRL-Txt.

The three stations R3, Agdal and Agafay are located in croplands that are intensively irrigated all year long. One can question a possible modulation of the local meteorological fields by the irrigation process and therefore question the importance of accounting for irrigation in models to simulate the near-surface climate in the Haouz plain. Although parameterizations of irrigation have been developed for ORCHIDEE (e.g., De Rosnay, 2003; Arboleda et al., 2023), none is operational when ORCHIDEE is coupled to LMDZ and therefore applicable in our simulations.

To assess whether accounting for irrigation may improve the simulations, we implemented a coarse and first-order parameterization to roughly represent the effect of the drip irrigation on the soil moisture over the Haouz plain crops. The parameterization has been activated between the longitudes -8.5 and -7.5 and the latitudes 31.5 and 31.7 that is, an area encompassing the Haouz plains cropland surrounding the three stations (see figure S2 in the supplement). It consists in nudging the soil moisture SM within the 10 cm below the surface towards the saturated value of SMs when SM drops below a fraction x1 of SMs (see figure S3 in the supplement)

$$\frac{dSM}{dt} = -\frac{SM - SM_S}{\tau} \quad (7)$$

With τ is a typical time scale, dt is the surface model time scale. The nudging stops when SM becomes greater than x_2 SM_s. x_1 and x_2 were set to 0.2 and 0.8 for our sensitivity experiments. We further set $\tau = 6h$ since it is a reasonable time scale for the near-surface soil to be humidified during drip irrigation over the Haouz plain. Note that the nudging formulation of Eq. 7 does not enable us to capture the exact timing of irrigation events. Importantly, this parameterization does not intend to be an effective and detailed irrigation parameterization, but a 1st order approach to assess 1st order effects.

(a)

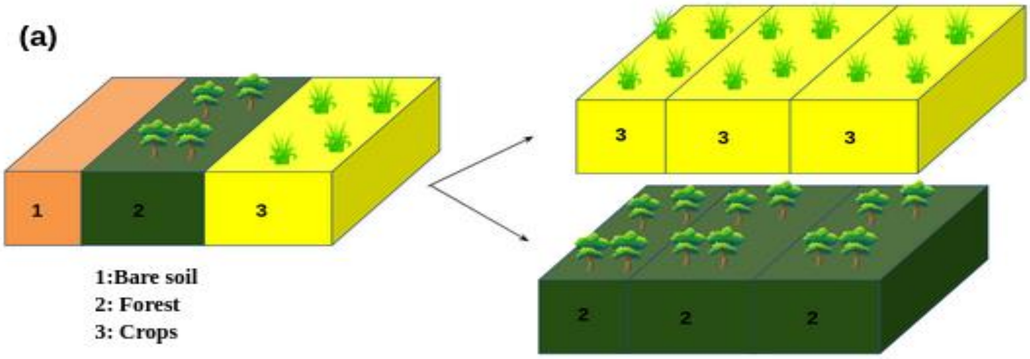

(b)

R3 (Wheat)	Bare soil: 12% Forest: 17% Crops: 71%
Agdal (Olive)	Bare soil: 25% Forest: 3% Crops: 72%
Agafay (Orange)	Bare soil: 33% Forest: 0.5% Crops: 66%

R3 (Wheat)	Wheat: 100%
Agdal (Olive)	Forest: 100%
Agafay (Orange)	Forest: 100%

Figure 3 Overview of the ORCHIDEE default grid cell land cover (a) and the updated one consisting of 100% of Forest in Agdal and Agafay and Crops in R3. The percentage of each type of land cover in each station grid cell is listed in the table (b) as simulated by the model (left panel) and the adapted one (right panel).

d. Observation-model comparison

Model evaluation is performed by comparing each station data to the nearest model grid point output (right panel in Fig.1). To take into consideration each station's elevation mismatch with its corresponding model grid box in model-observations comparisons, we use a moist lapse rate of 6.5 K km^{-1}. For wind speed, as the observation height is less than 10m (Table 1). We extrapolate the simulated 10-m wind speed assuming a logarithmic wind profile, based on the Monin-Obukhov Similarity theory in neutral conditions. The wind speed at a height h is given by:

$$U(h) = \frac{\log\left(\frac{h}{z_{0m}}\right)}{\log\left(\frac{10}{z_{0m}}\right)} \times U_{10} \qquad (8)$$

Where z_{0m} is the aerodynamic roughness height, U is wind speed and U_{10} is the wind speed at 10m height. In addition, the fifth generation of the ECMWF Reanalysis (ERA5, Hersbach et al., 2020) is used to compare and discuss the model's performance with respect to a reanalysis product. Note that none of the LMI network data is assimilated by ERA5, but we include it in our analysis as it serves as a reference dataset frequently used for climate assessment in Morocco.

The observed surface albedo is calculated as the ratio of the upward radiation to the downward surface radiation above the canopy between 08h and 17h LT. Reference observed surface temperature is calculated from downward and upward longwave radiative flux measurements above the canopy using the Stefan-Boltzman law and assuming a surface emissivity value of 1.

Furthermore, an evaluation of the simulated aerodynamic roughness height z_{0m} is also conducted by comparing it with observations. These latter are estimated using sonic anemometer measurements of the wind speed and friction velocity u* and applying the MO similarity theory for wind speed profile:

$$U(z) = \frac{u^*}{\kappa}\left[\ln\left(\frac{z-d}{z_{0m}}\right) - \Psi\left(\frac{z-d}{L}\right)\right] \qquad (9)$$

where z is the measurement height, d is the displacement height, assumed equal to 2/3 of the canopy height (Foken, 2008). L is the MO length (Monin & Obukhov, 1954) and Ψ is the integral of the stability function for momentum (Foken, 2008). Note that the evaluation of the roughness height is challenging, since the measured z_0 may include contributions from upstream areas advected at the measurement site, which is not accounted for in the model (Fesquet et al., 2009). As MO theory is strictly valid in stationary and near-neutral conditions, a pre-selection of the wind data has been performed following Vignon et al., 2017 (see their Appendix A). In Agdal, given the station's position within the orchards (Ezzahar et al., 2007), we considered the measurements corresponding only to northerly and north-westerly winds.

Unfortunately, no observational values for z_{0h} could be properly estimated. In fact, determining reliable z_{0h} from single sonic anemometer measurements is delicate since on one hand, the estimation errors in near-neutral conditions are large and on the other hand, z_{0h} values estimated far from neutrality are strongly dependent on the choice of the stability functions (Vignon et al., 2017).

3. Results and discussion

In this section, we firstly evaluate the model outputs from the STD simulation and then discuss the model-observation comparison with updated land cover before running different sensitivity tests to explore the main identified biases.

a. Near surface meteorological fields

1) Overview analysis of the STD simulation

Observed and simulated mean diurnal cycles of averaged near-surface temperature (T), relative humidity (RH) and wind speed (U) are compared at the three stations: Agdal, R3 and Agafay (Fig. 4). The ERA5 reanalysis is also plotted as an indication. In this paragraph, the analysis will focus on the model STD simulation (orange curves in Fig. 4).

The observed minimum temperature occurs around 5:30 local time (LT) – 7:30 LT and the maximum around 15:30 LT. The average diurnal temperature range is around 12°C in R3 (Fig. 4.d) and reaches 15°C in Agdal and Agafay (Figs. 4.a, 4.g). The lower diurnal temperature in R3 when compared to the other stations is explained by the considered season at this station (winter & spring). Let's recall that the time periods considered for each station are different (Sect. 2.a). The daytime temperature is well captured by the model while ERA5 reanalysis exhibits a cold bias that reaches 4 K in the afternoon in Agdal. Saouabe et al. (2022) also reported a similar bias in air temperature in a 53-year study period from 1967 to 2020 over Tensift basin. Nighttime temperature is well simulated in Agdal with differences less than 0.5 K. However, the model shows a pronounced warm (+2 K) nocturnal bias in R3 and Agafay, which leads to an underestimated diurnal temperature range.

The relative humidity signal reflects that of the temperature and LMDZ-ORCHIDEE exhibits a pronounced low bias during night-time. Differences with observations range from -12 to - 20%. ERA5 fits well the observed RH during nights in Agdal and R3, however, an underestimation emerges during daytime at R3 and Agafay. The average diurnal cycles show also that the STD simulation overestimates wind speed during day and night in Agdal and Agafay (Figs

4.c, 4.i) with positive differences reaching 1.5 to 2.5 m/s. Daytime differences are strongest during summer (Fig. 5) and the maximum occurs around 19:00 LT. An opposite behavior is noticeable at R3 station (Fig. 4.f) with a wind speed that is underestimated by up to -1.5 m/s in the afternoon. Note that the land cover varies between the studied sites, with wheat in R3 and trees in Agafay and Agdal (oranges and olive orchards).

Note that the model-observation differences evidenced at R3 in terms of temperature, relative humidity and wind speed are qualitatively similar at the two other wheat-covered stations Graoua and Chichaoua. At this stage, it is difficult to know whether the model-observation differences are due to model physics shortcomings or to the representativeness of station observations with respect to the size of the corresponding mesh. Hence, we will now analyze the CTRL simulation in which the land cover is modified in the whole grid cell to better represent the vegetation type surrounding the corresponding station.

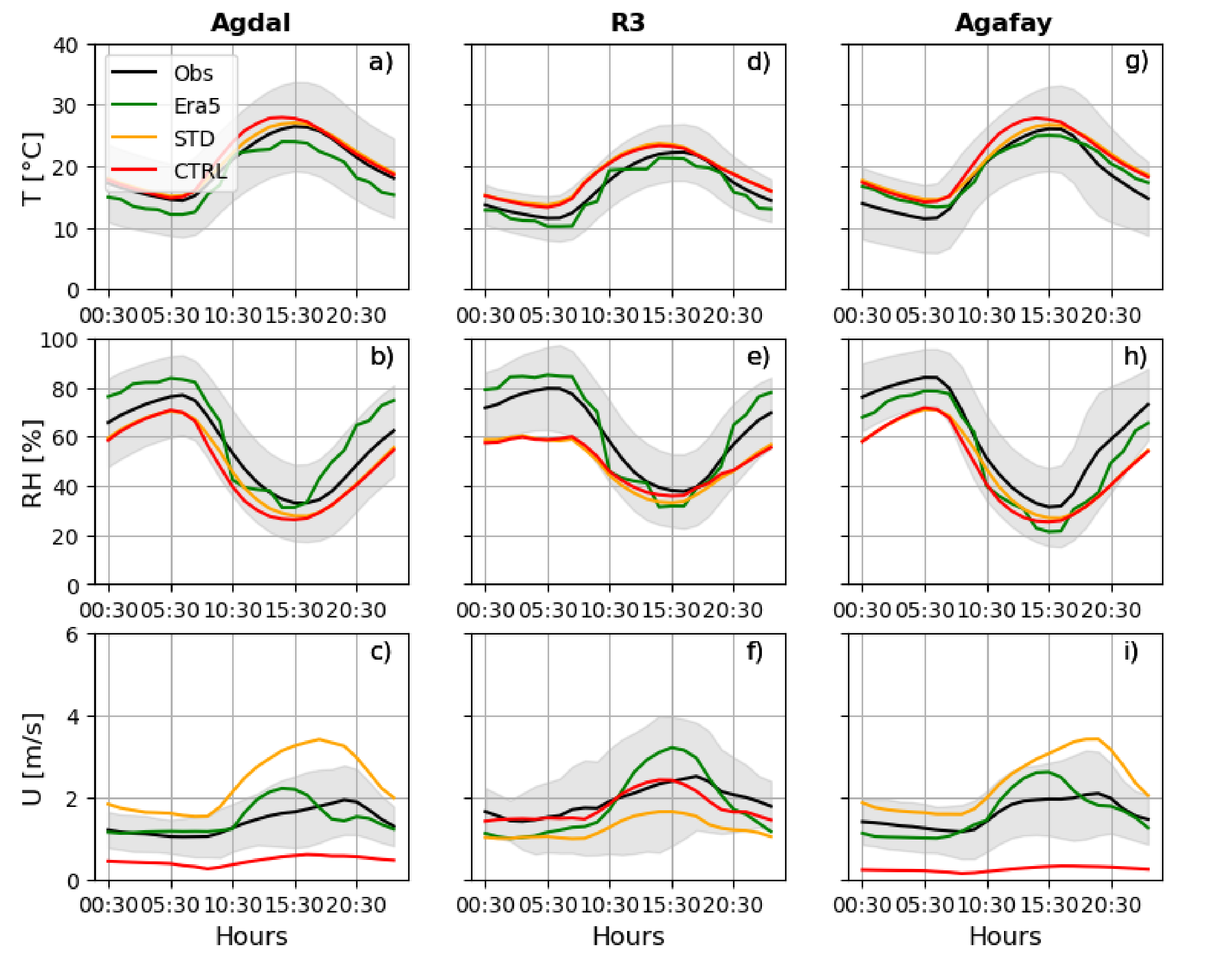

Figure 4 Mean diurnal cycle of T, RH and U over Agdal, R3 and Agafay stations. The black line shows observations, the orange line the standard simulation (STD), the red line the control simulation (CTRL) and the green one represents ERA5. Shadings denote the variability over the measurement period for each station (± σ). Note that the mean and standard deviation are calculated for each hour over the full measurement period for each station.

2) Analysis of the CTRL simulation with adapted land use for more consistent model-observation comparison

The comparison of the most relevant surface parameters for the surface-atmosphere coupling -namely the albedo and the roughness height - between the CTRL and STD simulations is given in Table 2.

Overall, a better agreement with observation in the CTRL set-up is noticeable for the two quantities. In particular, the CTRL simulation shows a closer-to-observation surface albedo value at the three sites owing to the removed bare soil fraction in the station grid cells, mainly in Agdal and Agafay where it was initially around 30% and then decreased by 50%.

The average diurnal cycle of T, RH and U of the updated land use simulation (CTRL) in Agdal, R3 and Agafay grid cells are shown in Fig. 4 (red curves). Overall, temperature and relative humidity show no significant change in the CTRL simulation wrt to STD at the three stations. Fig. 5 further shows the mean diurnal cycles separately for summer (JJA) and winter (DJF) seasons at Agafay station (similar figures for Agdal and R3 are provided in the supplementary material: Figs. S4 & S5). While T and RH show no substantial differences with the STD simulation, the wind speed in the CTRL simulation is significantly weaker and even underestimated at Agdal and Agafay stations. This is consistent with the much lower z_{0m} values in the CTRL configuration at these two stations. In the STD configuration, as the forest percentage only equals 3% and 1% in the Agdal and Agafay grid cells respectively, the mesh-averaged roughness height is much lower than the measured local one (Table 2). Conversely, the wind speed in CTRL is stronger at R3, where z_{0m} is higher than in the STD simulation for which the mesh-averaged roughness height is significantly higher than the observed one owing to a substantial forest percentage (17%) in the mesh. Overall the mean diurnal cycles of wind speed in CTRL are in better agreement with the local observations at R3 station than in STD (Fig. 4 and Fig 6).

Although the CTRL set-up has improved the model-observation comparison, substantial biases in the simulation of the near-surface temperature, humidity and wind remain. A comprehensive analysis of the surface energy budget is necessary to decipher the remaining model-observation differences.

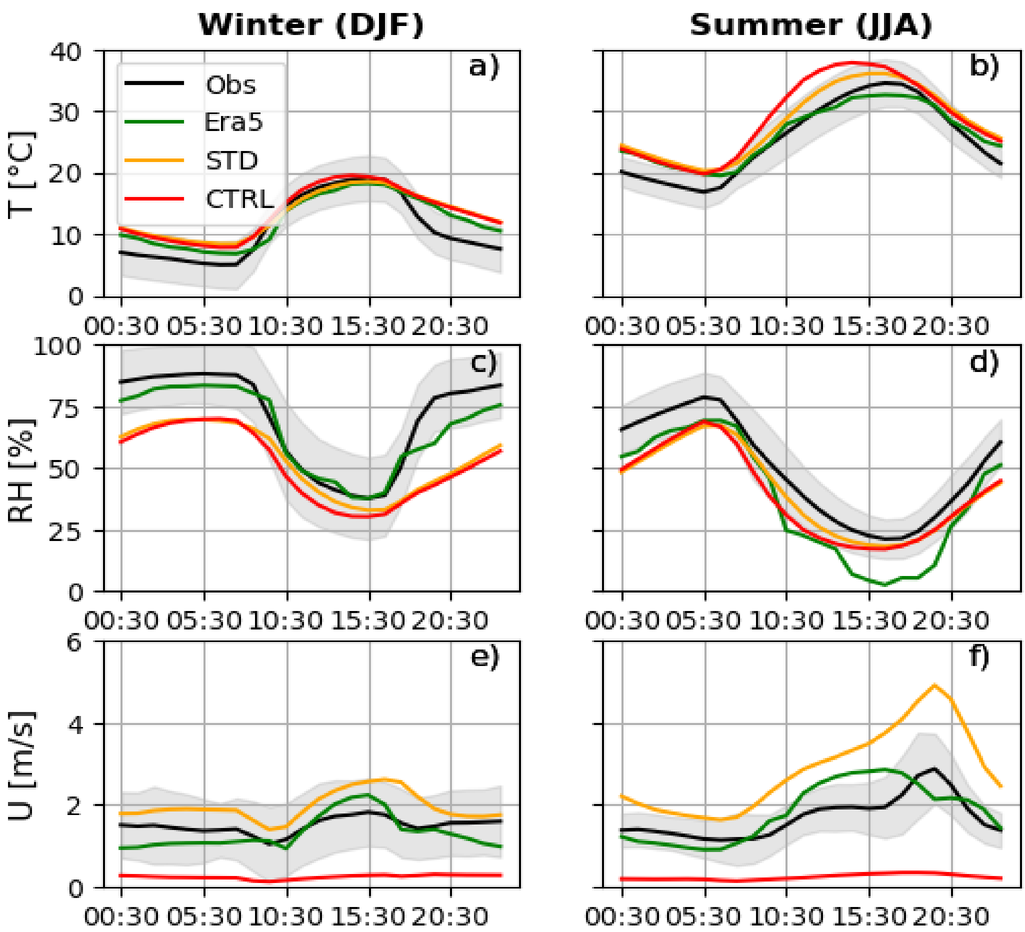

Figure 5 Mean diurnal cycle of T, RH and U during winter (DJF) and summer (JJA) for 2006-2009 period at Agafay station. The black line shows observations, the orange line the standard simulation (STD), the red line the control simulation (CTRL) and the green one represents ERA5. Shadings denote the variability over the measurement period for each station (± σ). Note that the mean and standard deviation are calculated for each hour over the full measurement period for each station.

410

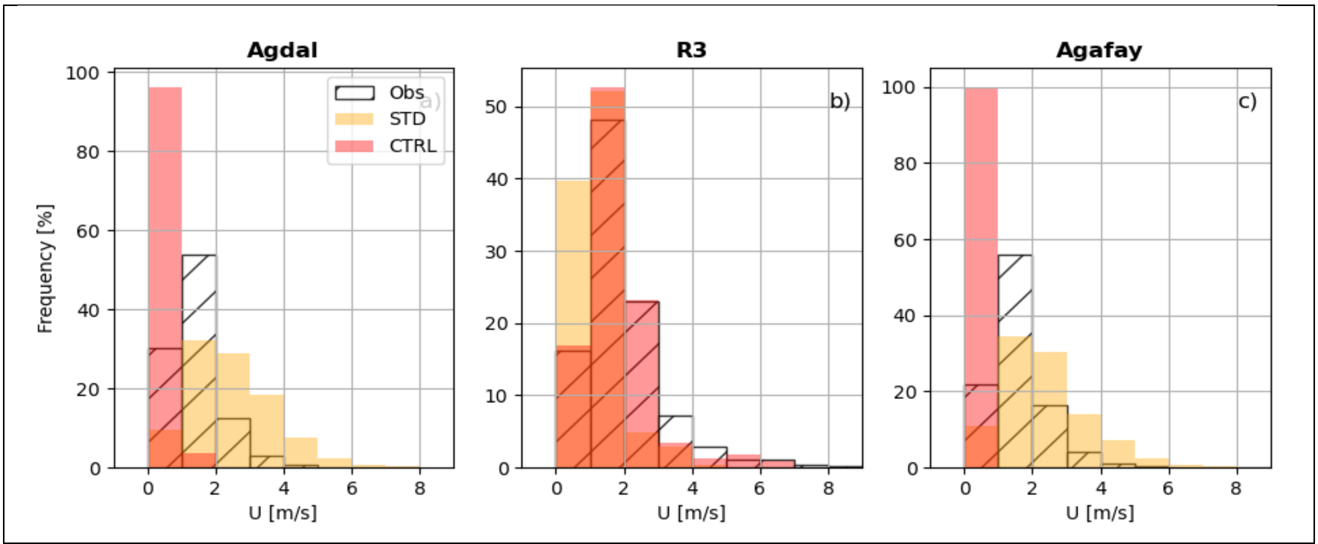

Figure 6 Wind speed distribution in observations (black hatches), STD (orange) and CTRL (red) simulations over Agdal (a), R3 (b) and Agafay (c) stations.

	z_{0m} [m]			Albedo		
Station	**Obs**	**STD**	**CTRL**	**Obs**	**STD**	**CTRL**
Agdal	1.26 (0.76)	0.02 (0.03)	1.42 (10^{-3})	0.11 (0.02)	0.25 (0.01)	0.12 ($4 .10^{-3}$)
R3	0.02 (0.07)	0.32 (0.01)	0.10 (1.10^{-4})	0.19 (0.04)	0.16 (3.10^{-3})	0.17 ($3 .10^{-3}$)
Agafay	0.10 (0.28)	0.01 (6.10^{-3})	1.39 (10^{-2})	0.16 (0.03)	0.29 (7.10^{-3})	0.14 (0.01)

Table 2 Observed and simulated albedo and roughness height (median value and interquartile range in brackets). As z_{0m}spans several orders of magnitude, the median of $z_{0m}$is calculated as the median of the distribution of the logarithmic values i.e. the exponential of the median of $\log(z_{0m})$.

b. Analysis of the surface energy balance and surface temperature

The diurnal cycles of the observed (Obs) and simulated (CTRL) surface energy balance over the studied stations are shown in Fig. 7. Results from the STD simulation are presented in the supplementary material (Fig S6). During daytime, incoming solar radiation reaches a maximum value of 800 to 900 W m-2 in the model. These values are higher than those observed suggesting a possible underestimated cloud cover in the simulation. Longwave radiative fluxes are well represented overall the studied sites, although, an overestimated daytime LW_{up} is noticeable, following the surface temperature (Ts) signal. Fig. 8 evidences a strong overestimation of Ts during daytime with differences wrt observations exceeding 5°C. During nighttime, Ts is reasonably well simulated at the two tree-filled sites Agafay and Agdal, but it is overestimated at R3 by nearly 2°C. At Agdal and Agafay, the simulated latent heat flux is underestimated by more than 100 W m^{-2} during daytime compared with observations. Conversely, the daytime sensible heat flux is overestimated in amplitude, with a bias exceeding 100 W m^{-2} at Agdal and Agafay at noon. At R3, a similar pattern is noticeable but the amplitude of the biases are reduced compared to the two other stations. Overall, the strong overestimation of the Bowen ratio - i.e. the ratio between the sensible and latent heat fluxes -associated with too warm day time temperatures at the three sites may suggest an underestimation of the soil moisture leading to a deficit in evapo-transpiration. This aspect will be further discussed in Sect. 3.d.

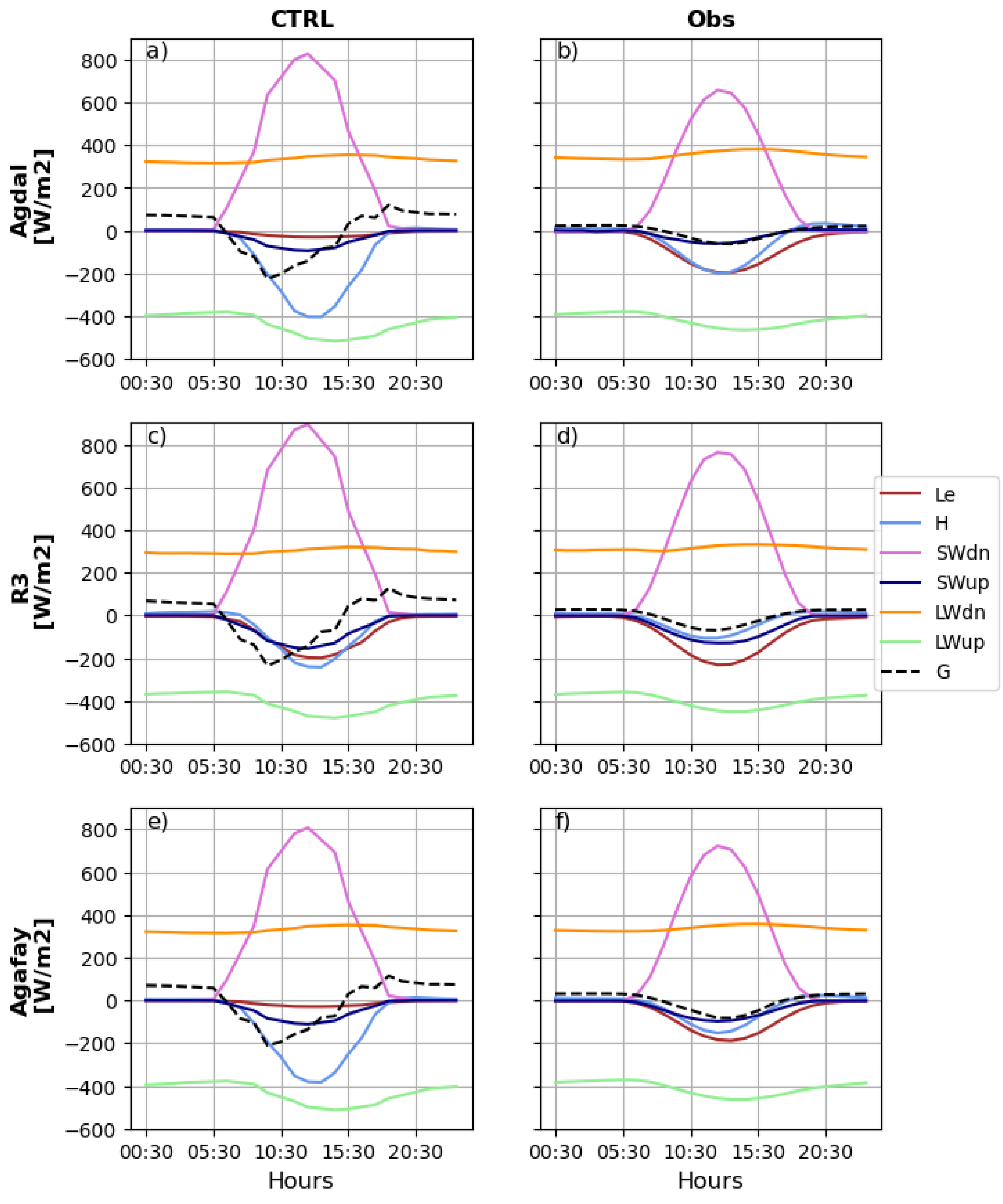

Figure 7 Average diurnal cycle of downward (SWdn) and upward (SWup) shortwave radiative fluxes, downward (LWdn) and upward (LWup) longwave radiation, the sensible (H) and latent heat fluxes (Le) and the ground heat flux (G) at Agdal (upper panel), R3 (middle panel) and Agafay (lower panel) stations. The left panel represents CTRL simulation and the right one represents observations. Fluxes are defined positive towards the surface.

435

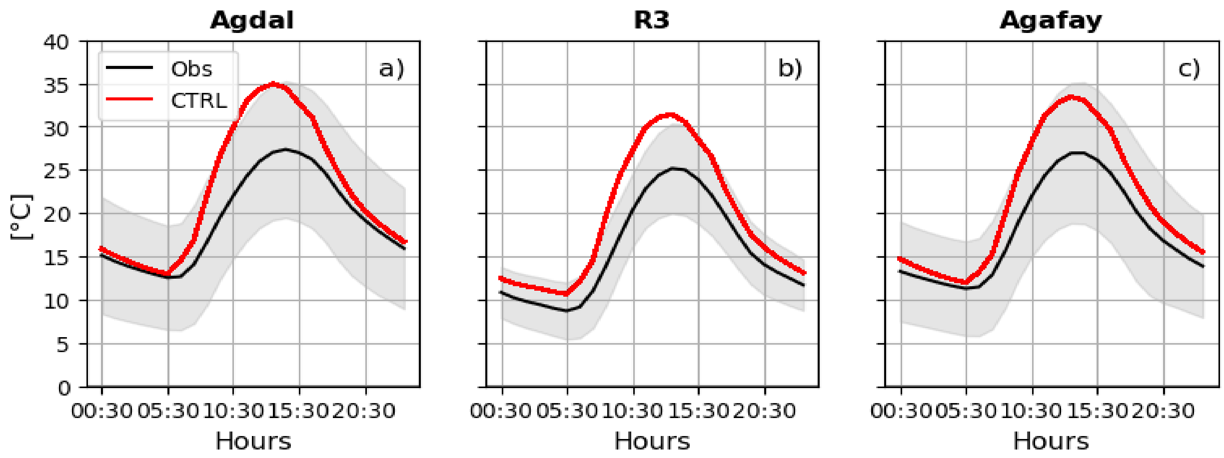

Figure 8 Observed (black curves) and simulated (red curves) surface temperature (solid lines) in Agdal, R3 and Agafay stations. Vertical bars denote the standard deviation around the observations' average value. Shadings denote the variability over the measurement period for each station (± σ). Note that the mean and standard deviation are calculated for each hour over the full measurement period for each station.

c. Investigation of the near-surface warm and dry nocturnal biases at R3 and Agafay

Amongst the remaining biases in the CTRL simulation, a warm bias at 2 m coinciding with an underestimation of the relative humidity is noticeable at R3 and Agafay stations (Fig 4). At R3, the overestimated nocturnal air temperature is associated with an overestimated surface temperature (Fig. 8b) which is mostly attributed to an overestimation of the nighttime ground heat flux (Fig 7c). The latter can be explained by the strong overestimation of the daytime surface temperature and ground heat flux and to the subsequent excess in heat storage in the soil. This aspect is further investigated in the next section.

The explanation of the nocturnal warm bias at R3 also holds for Agafay station (see Fig 7.e.f and 8.c) However, a strong overestimation of the surface-based temperature inversion (Ta - Ts) is also noticeable at the latter station (see red line in Fig 9c) thereby questioning the representation of the surface-atmosphere thermal coupling. The thermal coupling is controlled by the intensity of the surface turbulent sensible heat flux whose amplitude is underestimated during nighttime in the CTRL simulation at Agafay (Table 3). Such an underestimation can be - at least partly - explained by the underestimation of the near surface wind speed at Agafay in the CTRL simulation (Fig. 4i) and linked to an overestimation of the surface wind drag. The latter strongly depends on the roughness of the terrain which is parameterized with the momentum (z_{0m}) and thermal roughness heights (z_{0h}), see Eq. 5. Table 2 shows that the z_{0m} in the CTRL simulation - which depends on the LAI following Eq. 1 - is significantly overestimated at Agafay compared to observations. We have therefore performed a sensitivity test (CTRL-z0 simulations) in which we prescribe the z0 values. We set z_{0m} to the mean observed value (Table 2) for each station grid point and prescribe $z_{0h}=z_{0m}/10$ ratio that is commonly used for uniformly vegetated surfaces (e.g. Sandu et al., 2012). The new values of z_{0m} and z_{0h} are shown in Table 3. In this new simulation (CTRL-z0), we obtained a more realistic wind speed (see blue line in Fig. 9c), albeit slightly underestimated during nighttime, with differences lower than 0.25 m s^{-1}. However, the biases in nighttime 2-m temperature and relative humidity as well as the amplitude of the surface-based temperature inversion are only slightly reduced (Fig. 9.a, b, d). It is worth noting that the surface temperature remains similar between CTRL-z0 and CTRL (not shown).

Increasing the value of z_{0h} (or the ratio z_{0h}/z_{0m}) may help further enhance the intensity of the thermal coupling and reduce the amplitude of the surface-based inversion but calibrating more precisely this parameter in our case is delicate since we do not have any reliable observational reference.

	z_{0m} [m]			**z_{0h} [m]**		**H [W m^{-2}]**		
Statistics	**Obs**	**CTRL**	**CTRL-z0**	**CTRL (10^{-4})**	**CTRL-z0**	**Obs**	**CTRL**	**CTRL-z0**
Median (q3-q1)	0.10 (0.39)	1.39 (0.01)	0.14 (0.03)	5.8 (0.6)	0.01 (0.003)	-5.84 (5.59)	-3.54 (7.01)	-3.16 (6.07)

Table 3: Median and interquartile values of dynamical and thermal roughness length, and sensible heat flux at 01:30 LT as simulated by STD, CTRL and CTRL-z0 configurations in Agafay station. As z_{0m} and z_{0h} span several orders of magnitude, their median is calculated as the median of the distribution of the logarithmic values i.e. the exponential of the median of $\log(z_{0m})$ and $\log(z_{0h})$ respectively.

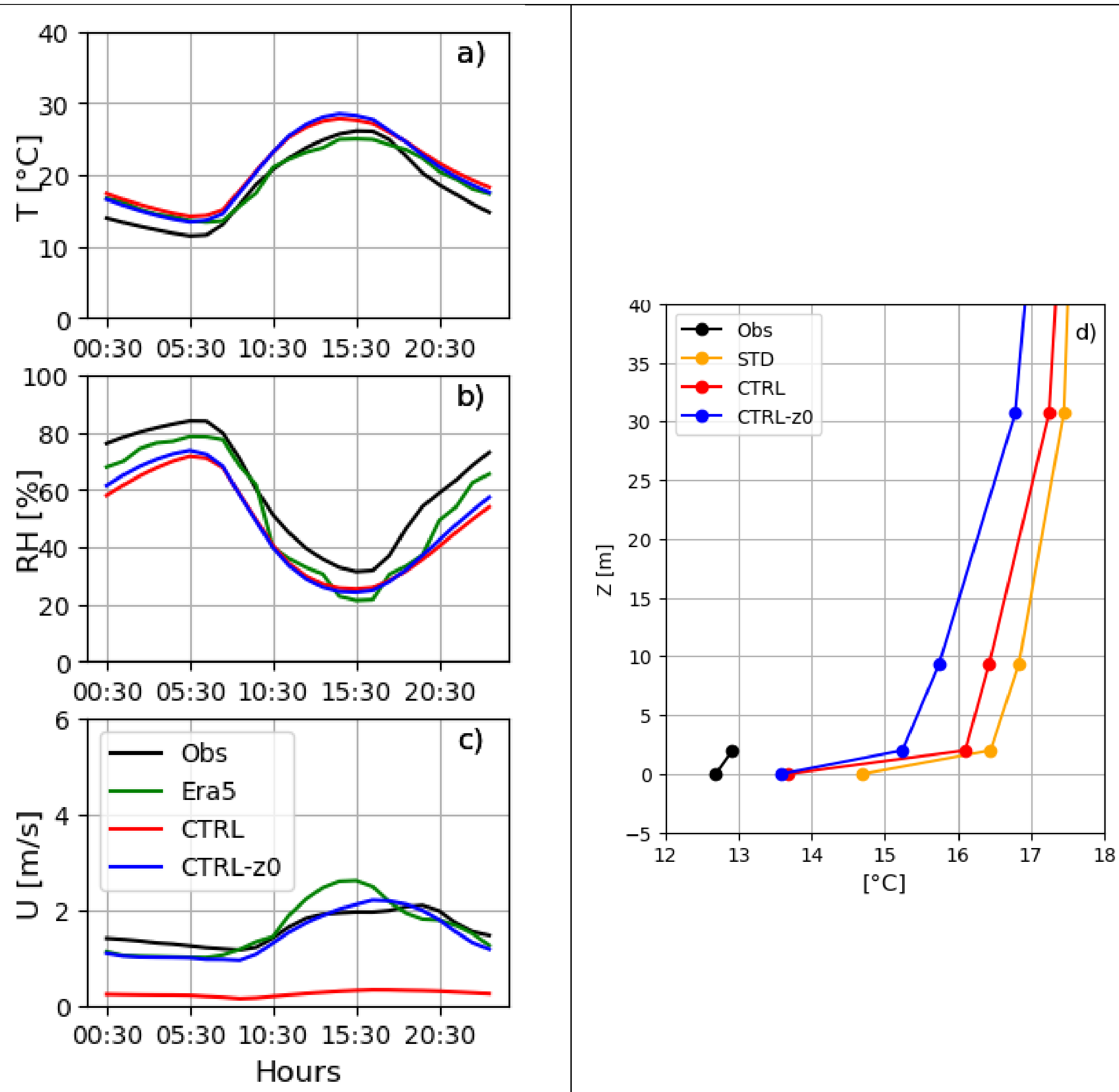

Figure 9: Mean diurnal cycle of T (panel a), RH (b) and U (c), with near-surface vertical profiles of temperature over Agafay station at 01:30 LT (d). The black line shows observations, the red line the control simulation (CTRL), the blue line the simulation with prescribed z_0 (CTRL-z0) and the green one shows ERA5.

d. Investigation of the surface dry bias and diurnal warm bias

The most pronounced biases that remains in the CTRL and CTRL-z0 simulations at the three stations is the low bias in RH and evaporation, the overestimation of the daytime surface temperature, as well as the overestimation of the Bowen ratio i.e. the ratio between the sensible heat flux (H) over latent heat flux (Le) during daytime. Such bias is associated with a deficit in soil moisture (Fig. 10), which itself may result from an underestimation of the input of soil water, namely precipitation and/or irrigation. Rainfall is relatively well captured near the Atlas piedmont at R3 but it is underestimated at Agafay and Agdal during the entire study period (Table 4). Differences in winter precipitation - which mostly originates from large-scale weather systems - exceed 0.7 mm/day at Agafay, and reach 0.3 mm/day at Agdal. Investigating the origin of the winter precipitation bias is beyond the scope of the present study and exploring the ability of LMDZ-ORCHIDEE to reproduce the main circulation patterns that drive precipitation in Morocco is tackled in Bahlane et al. (to be submitted). During summer, differences in precipitation vary from - 0.04 in Agafay to - 0.3 mm/day at Agdal. It is worth mentioning that summer precipitation events in the Haouz plain are mostly related to the development of deep wet convective systems over the High Atlas Mountains (thunderstorms or showers) that propagate over the plain in a second phase. The model simulates reasonable convective precipitation in summer but it remains localized over the high Atlas, particularly to the north of the Haouz plain (See Fig. S7). Despite an elaborated triggering scheme (Rio et al., 2013; Rochetin et al., 2014), the deep convection parameterization in LMDZ does not allow for the horizontal propagation of deep convective systems from one mesh to its neighbor. This can be particularly detrimental for simulations with horizontal resolutions around a few tens of kms and may explain part of the lack of precipitation over the plain in our simulations.

However, the deficit in precipitation cannot completely explain the underestimation of near-surface soil moisture throughout the year (see Fig. 10) which is noticeable at the three stations. Let's recall that the Haouz plain is an agricultural region with intensive use of irrigation. In a study based on simulations with the IPSL model, Mizuochi et al. (2021) show that irrigated zones are regions where the model biases in terms of near-surface climate and water cycle are amplified owing to the complex hydrometeorological regime. We therefore analyze a new simulation (CTRL-moist) which is similar to CTRL-z0 but in which we activate the first-order irrigation parameterization presented in Sect. 2c.

Soil moisture at 5cm depth increases by up to 0.1 m3/m3 with respect to CTRL-z0 simulation (Fig. S7), and leads to an increase in latent heat flux by up to 70 W m-2 during daytime as well as decrease in sensible heat flux (Fig. 11). Similar results hold from R3 and Agafay stations (see Figs. S8 & S9).

The increase in evaporation results in cooler daytime surface and 2-m temperatures as well as higher relative humidity by up to 10% and a decrease in specific humidity by 1. 10^{-3} kg kg^{-1}. However, it does not help reduce the overestimation of SWdn which invites for a deeper evaluation of the model in the region in terms of convective boundary-layer dynamics and cloud parameterization. Further measurement systems giving access to vertical profiles of meteorological variables, such as radiosondes or remote-sensing instruments could help gain further insight into the thermo-dynamical structure of the boundary layer above the plain. Results also show an increase in local precipitation associated with the increase in evapotranspiration which may suggest a local recycling of water as already noticed for other arid areas (Cheruy et al., 2013; Koster et al., 2004). Overall, the results of this sensitivity test emphasize that the dry and warm bias at the surface and the underestimation of evapotranspiration at the station locations in our CTRL simulations is partly explained by a lack of an irrigation parameterization.

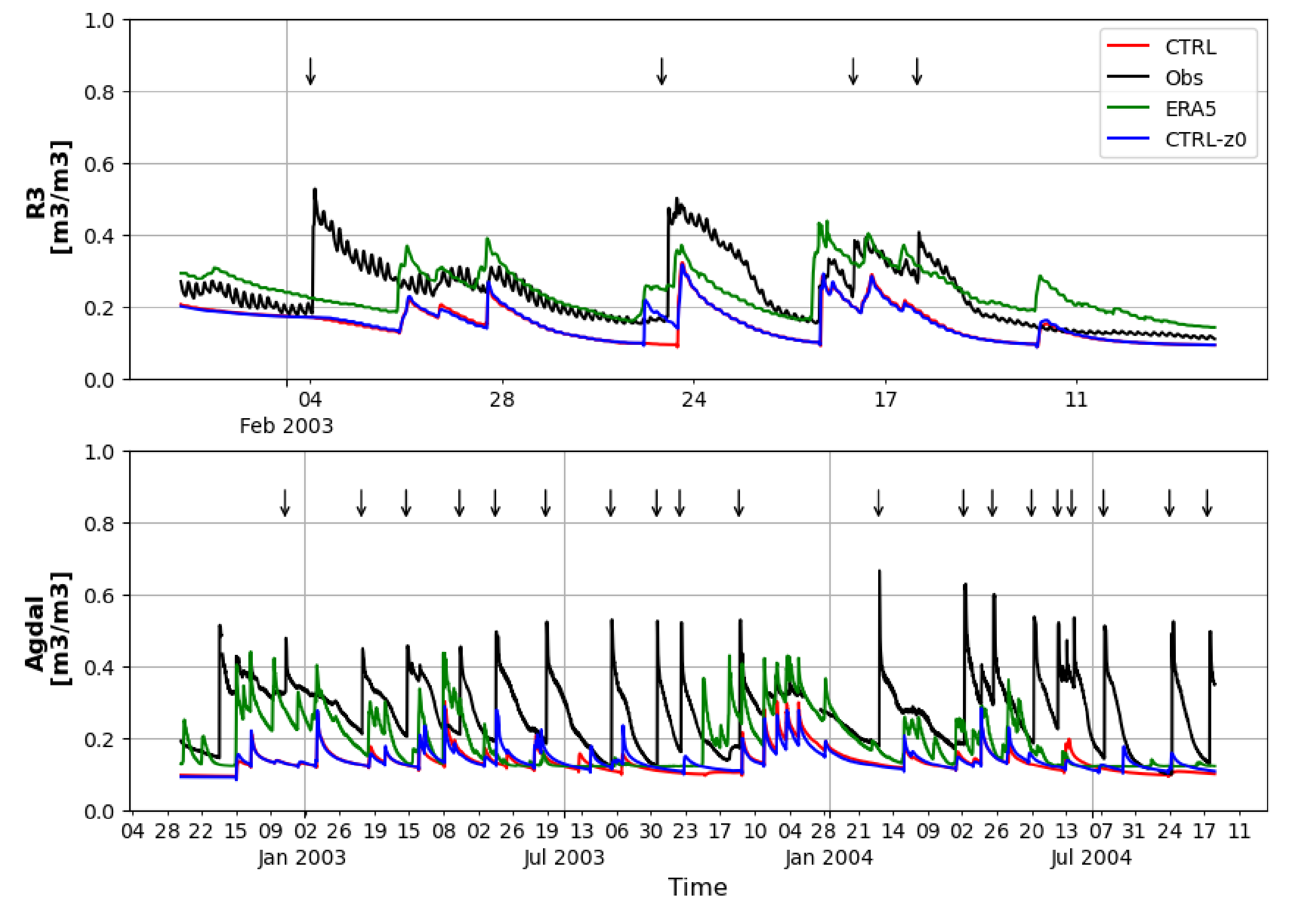

Figure 10: Soil moisture at 5 cm depth in R3 and Agafay stations grid cells for observations (black), ERA5 (green), CTRL (red) and CTRL-z0 (blue) simulation. The black arrows indicate the days with effective irrigation.

Total Average		**Agdal** (10/2002 - 11/2004)	**Agafay** (09/2006-12/2009)	**R3** /2003 - 05/2003)
Year	**Obs**	5.48	5.60	6.08
	STD	1.38	1.78	5.17
	CTRL	1.94	2.14	6.36

(10^{-1} mm	**CTRL-z0**	2.67	2.19	6.71
day^{-1})	**Era5**	4.15	3.02	5.38
	Obs	4.16	9.42	5.42
	STD	1.76	2.15	5.93
DJF	**CTRL**	1.76	2.02	6.78
(10^{-1} mm	**CTRL-z0**	2.12	2.75	6.44
day^{-1})	**Era5**	2.71	3.02	3.56
	Obs	4.27	1.51	-
	STD	0.51	1.31	-
JJA	**CTRL**	1.40	1.09	-
(10^{-1} mm	**CTRL-z0**	2.87	1.16	-
day^{-1})	**Era5**	0.28	0.65	-

Table 4 Observed and simulated annual and seasonal averaged precipitation at the three stations during the study periods. Note that no measurements for the JJA period are available at R3.

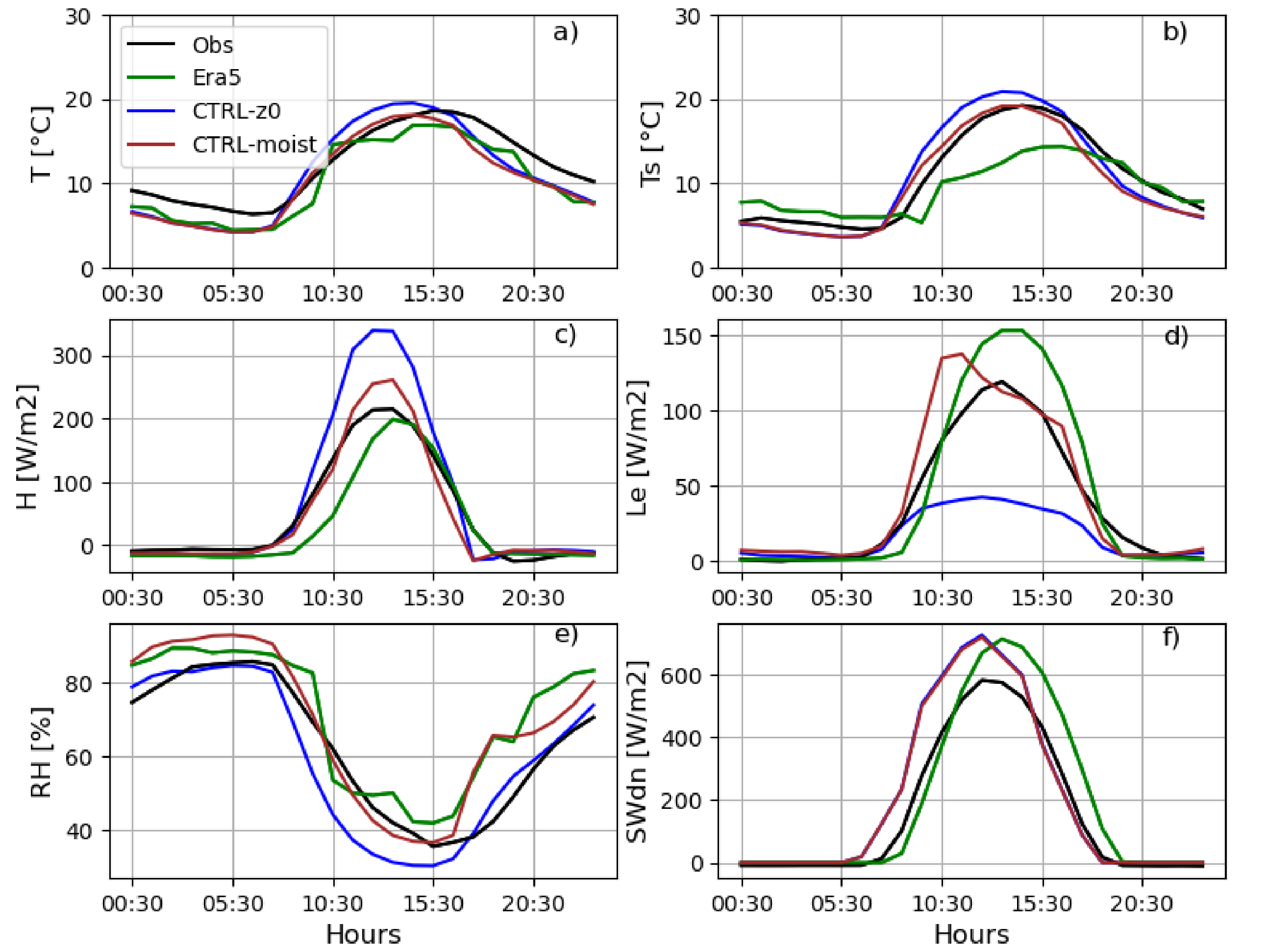

Figure 11 February 2003 evolution of Mean diurnal cycles of 2-m temperature T, surface temperature Ts, Le, H, SWdn and RH in Agdal station from model simulations (CTRL-z0 in blue and CTRL-moist in brown), ERA5 (green) and observations (black). Note that the time in the figures is in UTC time zone.

4. Summary and conclusions

The ability of climate models to simulate the near-surface climate is generally insufficiently assessed over Africa, particularly owing to the scarcity of meteorological observatories. This can question to a certain extent the climate projections over the continent, especially over the Maghreb, a hotspot of the current climate change which is experiencing a pronounced drying trend. In this paper, we use an original dataset of in situ meteorological observations collected over the Haouz plain in Morocco to assess the ability of LMDZ-ORCHIDEE GCM - the atmospheric and land surface component of the IPSL Coupled Model actively involved in the CMIP exercises - to simulate the near-surface climate and the land-atmosphere coupling in semi-arid agricultural

African plains. The model is run in a nudged and zoomed configuration which allows for a direct comparison between observations and simulations.

The analysis of the standard (STD) simulation revealed a 2-m nocturnal warm bias at R3 and Agafay, and a dry bias at all the stations as well as an overestimation (resp. underestimation) of the wind speed at the tree-covered (resp. wheat crop covered) stations. However, it is difficult to conclude from such an analysis if the model-observation differences are due to genuine model physics shortcomings or to the non-representativeness of station observations with respect to the size of the corresponding mesh. Our control (CTRL) configuration , which incorporates specific land cover characteristics corresponding to each station's vegetation, exhibits similar 2-m nocturnal warm and dry biases over R3 and Agafay, but it shows a more realistic wind speed at R3 in the middle of wheat crop fields. At Agdal and Agafay - with olive and orange cultures respectively – the prescribed Evergreen Broadleaf forests PFT overcorrects the aerodynamic roughness heights and produces overly weak wind speeds.

The analysis of the surface energy budgets reveals i) an overestimation of the downward shortwave radiative flux pointing to a possible underestimation of cloud cover; ii) a strong underestimation of the turbulent latent heat flux coinciding with an overestimation of the sensible heat flux and too warm daytime skin surface temperatures. Further sensitivity experiments made it possible to identify the causes of the major remaining biases in our simulations that can be summarized as follows:

- The 2-m warm nocturnal bias at R3 station is attributed to the excess in daytime soil heating while a too strong nighttime thermal decoupling also explains part of the bias at Agafay. This point in fact questions the parameterization of the roughness height - and more generally of the surface drag - over Evergreen tree crops such as orange trees since neither parameters typical of low (C3 or C4) crops nor those of typical Evergreen high forest are appropriate.
- The overestimation of the daytime skin surface temperature and the lack of surface evapotranspiration are associated with a strong deficit in soil moisture over the three types of culture. The latter is partly explained by a lack of precipitation at Adgal and Agafay and by the absence of an effective irrigation parameterization in LMDZ-ORCHIDEE for the three sites.

In fact, enhancing the model's surface moisture through a nudging method mimicking roughly an irrigation process helps simulate a more realistic evapotranspiration flux and daytime skin surface temperatures. Running reliable regional scenario simulations and carrying out impact studies over Morocco with LMDZ-ORCHIDEE would benefit from using a more sophisticated irrigation parameterization such as the one proposed in Arboleda et al. (2023).

This study has identified and highlighted the processes that should be correctly parameterized to realistically capture the main feature of the near-surface climate over the Moroccan agricultural plains. However, a comprehensive evaluation of the boundary layer dynamics in this region including an analysis of its vertical structure could not be performed, thereby raising the need to deploy observational systems such as radiosoundings or remote-sensing instruments. Note that the Moroccan weather services do not operate any routine radiosonde station over the Haouz plain, the nearest station is located at Casablanca, 220 km north of Marrakech.

In a Moroccan climate study perspective, it is also worth mentioning that our study has not assessed the performance of IPSL-CM to simulate the large-scale circulation patterns that drive the Moroccan climate and in particular the precipitation. This aspect has recently been tackled in Balhane et al. (in revision). Furthermore, our work has stressed the difficulty of evaluating numerical simulations from a model whose meshes are composed of heterogeneous vegetation cover with in situ station data. Note that the ongoing MOSAI project (Modèles et Observations pour les Interactions entre la Surface et l'Atmosphère, https://anr.fr/Projet-ANR-20-CE01-0018) is tackling this issue, proposing original evaluation methods and revisiting the formulations of surface turbulent fluxes in heterogeneous meshes.

Acknowledgments.

This work is conducted in the context of Khadija Arjdal's doctoral program funded by Mohammed VI Polytechnic University (UM6P) in the framework of the UM6P and l'École Polytechnique de Paris (X) collaboration project on climate modeling. We gratefully thank the Laboratoire Mixte Internationale (LMI-TREMA) for providing station data used for model evaluation. Vincent Simonneaux, Jamal Ezzahar and Mohamed Kharrou are thanked for their useful insights and discussions about the instrumented sites and also for the opportunity to visit these sites. Simulations were performed using HPC resources from the IDRIS (Institut du Développement et des Ressources en Informatique Scientifique, CNRS, France), projects RCES A0140100239 and RLMD AD010107632R1. We are grateful to Frédéric Hourdin, Abderrahmane Idelkadi, Florian Raymond, Catherine Rio, Maëlle Coulon Decorzons and Saloua Balhane for constructive insights. We also gratefully thank Agnès Ducharne, Pedro Arboleda Obando, Pierre Tiengou and Yann Meurdesoif for enriching and fruitful discussions about the irrigation process and its parameterization. We also acknowledge support from the DEPHY research group, funded by CNRS/INSU and Météo-France.

Competing interest

The authors declare that they have no competing interests.

Data Availability Statement.

Observation data is available on request from the joint international laboratory (LMI TREMA: https://www.lmi-trema.ma). ERA5 data is available to download from the link https://cds.climate.copernicus.eu

The last version of the LMDZ source code can be downloaded freely from the LMDZ web site. The version used for the specific simulation runs for this paper is the "svn" release 3987 which can be downloaded and installed on a Linux computer by running the "install_lmdz.sh" script available at this site (http://www.lmd.jussieu.fr/~/pub:./install_lmdz.sh). The processing code used in this study is available from the authors on request (Khadija.Arjdal@um6p.ma).

References

Ait El Mekki, O., Laftouhi, N.-E., 2016. Combination of a geographical information system and remote sensing data to map groundwater recharge potential in arid to semi-arid areas: the Haouz Plain, Morocco. Earth Sci. Inform. 9, 465–479. https://doi.org/10.1007/s12145-016-0268-0

Aït- Mesbah, S., Dufresne, J.L., Cheruy, F., Hourdin, F., 2015. The role of thermal inertia in the representation of mean and diurnal range of surface temperature in semiarid and arid regions. Geophys. Res. Lett. 42, 7572–7580. https://doi.org/10.1002/2015GL065553

Ali, E., W. Cramer, J. Carnicer, E. Georgopoulou, N.J.M. Hilmi, G. Le Cozannet, and P. Lionello, 2022: Cross-Chapter Paper 4: Mediterranean Region. In: Climate Change 2022: Impacts, Adaptation and Vulnerability. Contribution of Working Group II to the Sixth Assessment Report of the Intergovernmental Panel on Climate Change [H.-O. Pörtner, D.C. Roberts, M. Tignor, E.S. Poloczanska, K. Mintenbeck, A. Alegría, M. Craig, S. Langsdorf, S. Löschke, V. Möller, A. Okem, B. Rama (eds.)]. Cambridge University Press, Cambridge, UK and New York, NY, USA, pp. 2233–2272, doi:10.1017/9781009325844.021.

Arboleda-Obando, P. F., Ducharne, A., Yin, Z., and Ciais, P.: Validation of a new global irrigation scheme in the land surface model ORCHIDEE v2.2, EGUsphere [preprint], https://doi.org/10.5194/egusphere-2023-1323, 2023

Arjdal, K., Driouech, F., Vignon, Chéruy, F., Manzanas, R., Drobinski, P., Chehbouni, A., and Idelkadi, A. (2023). Future of land surface water availability over the Mediterranean basin and North Africa: Analysis and synthesis from the CMIP6 exercise. Atmospheric Science Letters, page e1180, https://doi.org/10.1002/asl.1180

Balhane, S., F. Cheruy, F. Driouech, K. El Rhaz, A. Idelkadi, A. Sima, É. Vignon, P. Drobinski, A. Chehbouni (2023) Advancing the simulation of precipitation over Morocco in a GCM with resolution enhancement and empirical run-time bias corrections. [In revision for International Journal of Climatology]

Balhane, S., Driouech, F., Chafki, O., Manzanas, R., Chehbouni, A., Moufouma-Okia, W., 2021. Changes in mean and extreme temperature and precipitation events from different weighted multi-model ensembles over the northern half of Morocco. Clim. Dyn. https://doi.org/10.1007/s00382-021-05910-w

Bell, B.A., Hughes, P.D., Fletcher, W.J., Cornelissen, H.L., Rhoujjati, A., Hanich, L., Braithwaite, R.J., 2022. Climate of the Marrakech High Atlas, Morocco: Temperature lapse rates and precipitation gradient from piedmont to summits. Arct. Antarct. Alp. Res. 54, 78–95. https://doi.org/10.1080/15230430.2022.2046897

Betts, A.K., 2007. Coupling of water vapor convergence, clouds, precipitation, and land-surface processes: LAND-SURFACE-CLOUD PROCESSES. J. Geophys. Res. Atmospheres 112. https://doi.org/10.1029/2006JD008191

Born, K., Fink, A.H., Knippertz, P., 2010. I-5.2 Meteorological processes influencing the weather and climate of Morocco 15.

Born, K., Fink, A.H., Paeth, H., 2008. Dry and wet periods in the northwestern Maghreb for present day and future climate conditions. Meteorol. Z. 17, 533–551. https://doi.org/10.1127/0941-2948/2008/0313

Botta, A., Viovy, N., Ciais, P., Friedlingstein, P., Monfray, P., 2000. A global prognostic scheme of leaf onset using satellite data: GLOBAL PROGNOSTIC SCHEME OF LEAF ONSET. Glob. Change Biol. 6, 709–725. https://doi.org/10.1046/j.1365-2486.2000.00362.x

Boucher, O., Servonnat, J., Albright, A.L., Aumont, O., Balkanski, Y., Bastrikov, V., Bekki, S., Bonnet, R., Bony, S., Bopp, L., Braconnot, P., Brockmann, P., Cadule, P., Caubel, A., Cheruy, F., Codron, F., Cozic, A., Cugnet, D., D'Andrea, F., Davini, P., de Lavergne, C., Denvil, S., Deshayes, J., Devilliers, M., Ducharne, A., Dufresne, J.-L., Dupont, E., Éthé, C., Fairhead, L., Falletti, L., Flavoni, S., Foujols, M.-A., Gardoll, S., Gastineau, G., Ghattas, J., Grandpeix, J.-Y., Guenet, B., Guez, E., Lionel, Guilyardi, E., Guimberteau, M., Hauglustaine, D., Hourdin, F., Idelkadi, A., Joussaume, S., Kageyama, M., Khodri, M., Krinner, G., Lebas, N., Levavasseur, G., Lévy, C., Li, L., Lott, F., Lurton, T., Luyssaert, S., Madec, G., Madeleine, J.-B., Maignan, F., Marchand, M., Marti, O., Mellul, L., Meurdesoif, Y., Mignot, J., Musat, I., Ottlé, C., Peylin, P., Planton, Y., Polcher, J., Rio, C., Rochetin, N., Rousset, C., Sepulchre, P., Sima, A., Swingedouw, D., Thiéblemont, R., Traore, A.K., Vancoppenolle, M., Vial, J., Vialard, J., Viovy, N., Vuichard, N., 2020. Presentation and Evaluation of the IPSL-CM6A-LR Climate Model. J. Adv. Model. Earth Syst. 12, e2019MS002010. https://doi.org/10.1029/2019MS002010

Cavicchia, L., Scoccimarro, E., Gualdi, S., Marson, P., Ahrens, B., Berthou, S., Conte, D., Dell'Aquila, A., Drobinski, P., Djurdjevic, V., Dubois, C., Gallardo, C., Li, L., Oddo, P., Sanna, A., Torma, C., 2018. Mediterranean extreme precipitation: a multi-model assessment. Clim. Dyn. 51, 901–913. https://doi.org/10.1007/s00382-016-3245-x

Chehbouni, A., Escadafal, R., Dedieu, G., Errouane, S., Boulet, G., Duchemin, B., Mougenot, B., Sminonneaux, V., Seghieri, J., Timouk, F., 2003. A multidisciplinary program for assessing the sustainability of water resources in semi-arid basin in Morocco: SUDMED 14229.

Chehbouni, A., Escadafal, R., Duchemin, B., Boulet, G., Simonneaux, V., Dedieu, G., Mougenot, B., Khabba, S., Kharrou, H., Maisongrande, P., Merlin, O., Chaponnière, A., Ezzahar, J., Er- Raki, S., Hoedjes, J., Hadria, R., Abourida, A., Cheggour, A., Raibi, F., Boudhar, A., Benhadj, I., Hanich, L., Benkaddour, A., Guemouria, N., Chehbouni, A.H., Lahrouni, A., Olioso, A., Jacob, F., Williams, D.G., Sobrino, J.A., 2008. An integrated modelling and remote sensing approach for hydrological study in arid and semi- arid regions: the SUDMED Programme. Int. J. Remote Sens. 29, 5161–5181. https://doi.org/10.1080/01431160802036417

Cherif, S., Doblas-Miranda, E., Lionello, P., Borrego, C., Giorgi, F., Iglesias, A., Jebari, S., Mahmoudi, E., Moriondo, M., Pringault, O., Rilov, G., Somot, S., Tsikliras, A., Vila, M., & Zittis, G. (2020). Drivers of change. In: Climate and Environmental Change in the Mediterranean Basin – Current Situation and Risks for the Future. First Mediterranean Assessment Report [Cramer W, Guiot J, Marini K (eds.)] Union for the Mediterranean, Plan Bleu, UNEP/MAP, Marseille, France, 59-180.

Cheruy, F., Campoy, A., Dupont, J.-C., Ducharne, A., Hourdin, F., Haeffelin, M., Chiriaco, M., Idelkadi, A., 2013. Combined influence of atmospheric physics and soil hydrology on the simulated meteorology at the SIRTA atmospheric observatory. Clim. Dyn. 40, 2251–2269. https://doi.org/10.1007/s00382-012-1469-y

Cheruy, F., Ducharne, A., Hourdin, F., Musat, I., Vignon, É., Gastineau, G., Bastrikov, V., Vuichard, N., Diallo, B., Dufresne, J., Ghattas, J., Grandpeix, J., Idelkadi, A., Mellul, L., Maignan, F., Ménégoz, M., Ottlé, C., Peylin, P., Servonnat, J., Wang, F., Zhao, Y., 2020. Improved Near- Surface Continental Climate in IPSL- CM6A- LR by Combined Evolutions of Atmospheric and Land Surface Physics. J. Adv. Model. Earth Syst. 12. https://doi.org/10.1029/2019MS002005

Cheruy, F., Dufresne, J.L., Aït Mesbah, S., Grandpeix, J.Y., Wang, F., 2017. Role of Soil Thermal Inertia in Surface Temperature and Soil Moisture-Temperature Feedback: SOIL MOISTURE TEMPERATURE FEEDBACK. J. Adv. Model. Earth Syst. 9, 2906–2919. https://doi.org/10.1002/2017MS001036

Coindreau, O., Hourdin, F., Haeffelin, M., Mathieu, A., Rio, C., 2007. Assessment of Physical Parameterizations Using a Global Climate Model with Stretchable Grid and Nudging. Mon. Weather Rev. 135, 1474–1489. https://doi.org/10.1175/MWR3338.1

de Rosnay, P., 2003. Integrated parameterization of irrigation in the land surface model ORCHIDEE. Validation over Indian Peninsula. Geophys. Res. Lett. 30, 1986. https://doi.org/10.1029/2003GL018024

Diallo, F.B., Hourdin, F., Rio, C., Traore, A.-K., Mellul, L., Guichard, F., Kergoat, L., 2017. The Surface Energy Budget Computed at the Grid-Scale of a Climate Model Challenged by Station Data in West Africa: GCM FACING WEST AFRICA IN-SITU DATA. J. Adv. Model. Earth Syst. 9, 2710–2738. https://doi.org/10.1002/2017MS001081

Diffenbaugh, N.S., Giorgi, F., 2012. Climate change hotspots in the CMIP5 global climate model ensemble. Clim. Change 114, 813–822. https://doi.org/10.1007/s10584-012-0570-x

Douville, H., K. Raghavan, J. Renwick, R.P. Allan, P.A. Arias, M. Barlow, R. Cerezo-Mota, A. Cherchi, T.Y. Gan, J. Gergis, D. Jiang, A. Khan, W. Pokam Mba, D. Rosenfeld, J. Tierney, and O. Zolina, 2021: Water Cycle Changes. In Climate Change 2021: The Physical Science Basis. Contribution of Working Group I to the Sixth Assessment Report of the Intergovernmental Panel on Climate Change [Masson-Delmotte, V., P. Zhai, A. Pirani, S.L. Connors, C. Péan, S. Berger, N. Caud, Y. Chen, L. Goldfarb, M.I. Gomis, M. Huang, K. Leitzell, E. Lonnoy, J.B.R. Matthews, T.K. Maycock, T. Waterfield, O. Yelekçi, R. Yu, and B. Zhou (eds.)]. Cambridge University Press, Cambridge, United Kingdom and New York, NY, USA, pp. 1055–1210, doi:10.1017/9781009157896.010.

Driouech, F., 2010. Distribution des précipitations hivernales sur le Maroc dans le cadre d’un changement climatique : descente d’échelle et incertitudes.

Driouech, F., Déqué, M., Mokssit, A., 2009. Numerical simulation of the probability distribution function of precipitation over Morocco. Clim. Dyn. 32, 1055–1063. https://doi.org/10.1007/s00382-008-0430-6

Driouech, F., ElRhaz, K., Moufouma-Okia, W., Arjdal, K., Balhane, S., 2020. Assessing Future Changes of Climate Extreme Events in the CORDEX-MENA Region Using Regional Climate Model ALADIN-Climate. Earth Syst. Environ. 4, 477–492. https://doi.org/10.1007/s41748-020-00169-3

Drobinski, P., Da Silva, N., Bastin, S., Mailler, S., Muller, C., Ahrens, B., Christensen, O.B., Lionello, P., 2020. How warmer and drier will the Mediterranean region be at the end of the twenty-first century? Reg. Environ. Change 20, 78. https://doi.org/10.1007/s10113-020-01659-w

Drobinski, P., Silva, N.D., Panthou, G., Bastin, S., Muller, C., Ahrens, B., Borga, M., Conte, D., Fosser, G., Giorgi, F., Güttler, I., Kotroni, V., Li, L., Morin, E., Önol, B., Quintana-Segui, P., Romera, R., Torma, C.Z., 2018. Scaling precipitation extremes with temperature in the Mediterranean: past climate assessment and projection in anthropogenic scenarios. Clim. Dyn. 51, 1237–1257. https://doi.org/10.1007/s00382-016-3083-x

Duchemin, B., Hadria, R., Erraki, S., Boulet, G., Maisongrande, P., Chehbouni, A., Escadafal, R., Ezzahar, J., Hoedjes, J.C.B., Kharrou, M.H., Khabba, S., Mougenot, B., Olioso, A., Rodriguez, J.-C., Simonneaux, V., 2006. Monitoring wheat phenology and irrigation in Central Morocco: On the use of relationships between evapotranspiration, crops coefficients, leaf area index and remotely-sensed vegetation indices. Agric. Water Manag. 79, 1–27. https://doi.org/10.1016/j.agwat.2005.02.013

Ducoudré, N.I., Laval, K., Perrier, A., 1993. SECHIBA, a New Set of Parameterizations of the Hydrologic Exchanges at the Land-Atmosphere Interface within the LMD Atmospheric General Circulation Model. J. Clim. 6, 248–273. https://doi.org/10.1175/1520-0442(1993)006<0248:SANSOP>2.0.CO;2

Er-Raki, S., Chehbouni, A., Khabba, S., Simonneaux, V., Jarlan, L., Ouldbba, A., Rodriguez, J.C., Allen, R., 2010. Assessment of reference evapotranspiration methods in semi-arid regions: Can weather forecast data be used as alternate of ground meteorological parameters? J. Arid Environ. 74, 1587–1596. https://doi.org/10.1016/j.jaridenv.2010.07.002

Er-Raki, S., Chehbouni, A., Guemouria, N., Duchemin, B., Ezzahar, J., Hadria, R., 2007. Combining FAO-56 model and ground-based remote sensing to estimate water consumptions of wheat crops in a semi-arid region. Agric. Water Manag. 87, 41–54. https://doi.org/10.1016/j.agwat.2006.02.004

Ezzahar, J., Chehbouni, A., Hoedjes, J.C.B., Er-Raki, S., Chehbouni, Ah., Boulet, G., Bonnefond, J.-M., De Bruin, H.A.R., 2007. The use of the scintillation technique for monitoring seasonal water consumption of olive orchards in a semi-arid region. Agric. Water Manag. 89, 173–184. https://doi.org/10.1016/j.agwat.2006.12.015

Fesquet, C., Drobinski, P., Barthlott, C., Dubos, T., 2009. Impact of terrain heterogeneity on near-surface turbulence structure. Atmospheric Res. 94, 254–269. https://doi.org/10.1016/j.atmosres.2009.06.003

Fink, A., Christoph, M., Born, K., et al. (2010). Climate. In: Speth, P., Christoph, M., Diekkrüger, B. (Eds.), Impacts of Global Change on the Hydrological Cycle in West and Northwest Africa. Springer, Heidelberg, pp. 54–58.

Foken, T., 2008. Micrometeorology. Springer, Berlin.

Gutiérrez, J.M., R.G. Jones, G.T. Narisma, L.M. Alves, M. Amjad, I.V. Gorodetskaya, M. Grose, N.A.B. Klutse, S. Krakovska, J. Li, D. Martínez-Castro, L.O. Mearns, S.H. Mernild, T. Ngo-Duc, B. van den Hurk, and J.-H. Yoon, 2021: Atlas. In Climate Change 2021: The Physical Science Basis. Contribution of Working Group I to the Sixth Assessment Report of the Intergovernmental Panel on Climate Change [Masson-Delmotte, V., P. Zhai, A. Pirani, S.L. Connors, C. Péan, S. Berger, N. Caud, Y. Chen, L. Goldfarb, M.I. Gomis, M. Huang, K. Leitzell, E. Lonnoy, J.B.R. Matthews, T.K. Maycock, T. Waterfield, O. Yelekçi, R. Yu, and B. Zhou (eds.)]. Cambridge University Press, Cambridge, United Kingdom and New York, NY, USA, pp. 1927–2058, doi:10.1017/9781009157896.021.

Garratt, J.R., Hicks, B.B., 1973. Momentum, heat and water vapour transfer to and from natural and artificial surfaces. Q. J. R. Meteorol. Soc. 99, 680–687. https://doi.org/10.1002/qj.49709942209

Harbouze, R., Pellissier, J.-P., Rolland, J.-P., Khechimi, W., 2019. Rapport de synthèse sur l’agriculture au Maroc (Recherche).

Hersbach, H., Bell, B., Berrisford, P., Hirahara, S., Horányi, A., Muñoz- Sabater, J., et al. (2020). The ERA5 global reanalysis. *Quarterly Journal of the Royal Meteorological Society*, *146*(730), 1999–2049. https://doi.org/10.1002/qj.3803

Hertig, E., 2004. Niederschlags- und Temperaturabschätzungen für den Mittelmeerraum unter anthropogen verstärktem Treibhauseffekt 288.

Hourdin, F., Couvreux, F., Menut, L., 2002. Parameterization of the Dry Convective Boundary Layer Based on a Mass Flux Representation of Thermals. J. Atmospheric Sci. 59, 1105–1123. https://doi.org/10.1175/1520-0469(2002)059<1105:POTDCB>2.0.CO;2

Hourdin, F., Foujols, M.-A., Codron, F., Guemas, V., Dufresne, J.-L., Bony, S., Denvil, S., Guez, L., Lott, F., Ghattas, J., Braconnot, P., Marti, O., Meurdesoif, Y., Bopp, L., 2013. Impact of the LMDZ atmospheric grid configuration on the climate and sensitivity of the IPSL-CM5A coupled model. Clim. Dyn. 40, 2167–2192. https://doi.org/10.1007/s00382-012-1411-3

Hourdin, F., Gueye, M., Diallo, B., Dufresne, J.-L., Escribano, J., Menut, L., Marticoréna, B., Siour, G., Guichard, F., 2015. Parameterization of convective transport in the boundary layer and its impact on the representation of the diurnal cycle of wind and dust emissions. Atmospheric Chem. Phys. 15, 6775–6788. https://doi.org/10.5194/acp-15-6775-2015

Hourdin, F., Jam, A., Rio, C., Couvreux, F., Sandu, I., Lefebvre, M., Brient, F., Idelkadi, A., 2019. Unified Parameterization of Convective Boundary Layer Transport and Clouds With the Thermal Plume Model. J. Adv. Model. Earth Syst. 11, 2910–2933. https://doi.org/10.1029/2019MS001666

Hourdin, F., Rio, C., Grandpeix, J., Madeleine, J., Cheruy, F., Rochetin, N., Jam, A., Musat, I., Idelkadi, A., Fairhead, L., Foujols, M., Mellul, L., Traore, A., Dufresne, J., Boucher, O., Lefebvre, M., Millour, E., Vignon, E., Jouhaud, J., Diallo, F.B., Lott, F., Gastineau, G., Caubel, A., Meurdesoif, Y., Ghattas, J., 2020. LMDZ6A: The Atmospheric Component of the IPSL Climate Model With Improved and Better Tuned Physics. J. Adv. Model. Earth Syst. 12. https://doi.org/10.1029/2019MS001892

Jam, A., Hourdin, F., Rio, C., Couvreux, F., 2013. Resolved Versus Parametrized Boundary-Layer Plumes. Part III: Derivation of a Statistical Scheme for Cumulus Clouds. Bound.-Layer Meteorol. 147, 421–441. https://doi.org/10.1007/s10546-012-9789-3

Jarlan, L., Khabba, S., Er-Raki, S., Le Page, M., Hanich, L., Fakir, Y., Merlin, O., Mangiarotti, S., Gascoin, S., Ezzahar, J., Kharrou, M.H., Berjamy, B., Saaïdi, A., Boudhar, A., Benkaddour, A., Laftouhi, N., Abaoui, J., Tavernier, A., Boulet, G., Simonneaux, V., Driouech, F., El Adnani, M., El Fazziki, A., Amenzou, N., Raibi, F., El Mandour, A., Ibouh, H., Le Dantec, V., Habets, F., Tramblay, Y., Mougenot, B., Leblanc, M., El Faïz, M., Drapeau, L., Coudert, B., Hagolle, O., Filali, N., Belaqziz, S., Marchane, A., Szczypta, C., Toumi, J., Diarra, A., Aouade, G., Hajhouji, Y., Nassah, H., Bigeard, G., Chirouze, J., Boukhari, K., Abourida, A., Richard, B., Fanise, P., Kasbani, M., Chakir, A., Zribi, M., Marah, H., Naimi, A., Mokssit, A., Kerr, Y., Escadafal, R., 2015. Remote

Sensing of Water Resources in Semi-Arid Mediterranean Areas: the joint international laboratory TREMA. Int. J. Remote Sens. 36, 4879–4917. https://doi.org/10.1080/01431161.2015.1093198

Khabba, S., Jarlan, L., Er-Raki, S., Le Page, M., Ezzahar, J., Boulet, G., Simonneaux, V., Kharrou, M.H., Hanich, L., Chehbouni, G., 2013. The SudMed Program and the Joint International Laboratory TREMA: A Decade of Water Transfer Study in the Soil-plant-atmosphere System over Irrigated Crops in Semi-arid Area. Procedia Environ. Sci. 19, 524–533. https://doi.org/10.1016/j.proenv.2013.06.059

Kharrou, M.H., Er-Raki, S., Chehbouni, A., Duchemin, B., Simonneaux, V., LePage, M., Ouzine, L., Jarlan, L., 2011. Water use efficiency and yield of winter wheat under different irrigation regimes in a semi-arid region. Agric. Sci. 02, 273–282. https://doi.org/10.4236/as.2011.23036

Koster, R.D., Suarez, M.J., Liu, P., Jambor, U., Berg, A., Kistler, M., Reichle, R., Rodell, M., Famiglietti, J., 2004. Realistic Initialization of Land Surface States: Impacts on Subseasonal Forecast Skill. J. Hydrometeorol. 5, 1049–1063. https://doi.org/10.1175/JHM-387.1

Lurton, T., Balkanski, Y., Bastrikov, V., Bekki, S., Bopp, L., Braconnot, P., Brockmann, P., Cadule, P., Contoux, C., Cozic, A., Cugnet, D., Dufresne, J., Éthé, C., Foujols, M., Ghattas, J., Hauglustaine, D., Hu, R., Kageyama, M., Khodri, M., Lebas, N., Levavasseur, G., Marchand, M., Ottlé, C., Peylin, P., Sima, A., Szopa, S., Thiéblemont, R., Vuichard, N., Boucher, O., 2020. Implementation of the CMIP6 Forcing Data in the IPSL‐ CM6A‐ LR Model. J. Adv. Model. Earth Syst. 12. https://doi.org/10.1029/2019MS001940

Marchane, A., Tramblay, Y., Hanich, L., Ruelland, D., Jarlan, L., 2017. Climate change impacts on surface water resources in the Rheraya catchment (High Atlas, Morocco). Hydrol. Sci. J. 62, 979–995. https://doi.org/10.1080/02626667.2017.1283042

Massman, W.J., 1999. A model study of kBΧH1 for vegetated surfaces using 'localized near-field' Lagrangian theory. J. Hydrol.

Meddi, M.M., Assani, A.A., Meddi, H., 2010. Temporal Variability of Annual Rainfall in the Macta and Tafna Catchments, Northwestern Algeria. Water Resour. Manag. 24, 3817–3833. https://doi.org/10.1007/s11269-010-9635-7

Mizuochi, H., Ducharne, A., Cheruy, F., Ghattas, J., Al-Yaari, A., Wigneron, J.-P., Bastrikov, V., Peylin, P., Maignan, F., Vuichard, N., 2021. Multivariable evaluation of land surface processes in forced and coupled modes reveals new error sources to the simulated water cycle in the IPSL (Institute Pierre Simon Laplace) climate model. Hydrol. Earth Syst. Sci. 25, 2199–2221. https://doi.org/10.5194/hess-25-2199-2021

Monin, A., Obukhov, A., 1954. Basic laws of turbulent mixing in the atmosphere near the ground. Tr. Geofiz Inst 163–187.

Nassah, H., Er-Raki, S., Khabba, S., Fakir, Y., Raibi, F., Merlin, O., Mougenot, B., 2018. Evaluation and analysis of deep percolation losses of drip irrigated citrus crops under non-saline and saline conditions in a semi-arid area. Biosyst. Eng. 165, 10–24. https://doi.org/10.1016/j.biosystemseng.2017.10.017

Raymond, F., Drobinski, P., Ullmann, A., Camberlin, P., 2018a. Extreme dry spells over the Mediterranean Basin during the wet season: Assessment of HyMeX/Med-CORDEX regional climate simulations (1979-2009). Int. J. Climatol. 38, 3090–3105. https://doi.org/10.1002/joc.5487

Raymond, F., Ullmann, A., Camberlin, P., Drobinski, P., Smith, C.C., 2016. Extreme dry spell detection and climatology over the Mediterranean Basin during the wet season: DRY SPELL OVER THE MEDITERRANEAN BASIN. Geophys. Res. Lett. 43, 7196–7204. https://doi.org/10.1002/2016GL069758

Raymond, F., Ullmann, A., Camberlin, P., Oueslati, B., Drobinski, P., 2018b. Atmospheric conditions and weather regimes associated with extreme winter dry spells over the Mediterranean basin. Clim. Dyn. 50, 4437–4453. https://doi.org/10.1007/s00382-017-3884-6

Raymond, F., Ullmann, A., Tramblay, Y., Drobinski, P., Camberlin, P., 2019. Evolution of Mediterranean extreme dry spells during the wet season under climate change. Reg. Environ. Change 19, 2339–2351. https://doi.org/10.1007/s10113-019-01526-3

Rio, C., Grandpeix, J.-Y., Hourdin, F., Guichard, F., Couvreux, F., Lafore, J.-P., Fridlind, A., Mrowiec, A., Roehrig, R., Rochetin, N., Lefebvre, M.-P., Idelkadi, A., 2013. Control of deep convection by sub-cloud lifting processes: the ALP closure in the LMDZ5B general circulation model. Clim. Dyn. 40, 2271–2292. https://doi.org/10.1007/s00382-012-1506-x

Rio, C., Hourdin, F., Couvreux, F., Jam, A., 2010. Resolved Versus Parametrized Boundary-Layer Plumes. Part II: Continuous Formulations of Mixing Rates for Mass-Flux Schemes. Bound.-Layer Meteorol. 135, 469–483. https://doi.org/10.1007/s10546-010-9478-z

Rochetin, N., Grandpeix, J.-Y., Rio, C., Couvreux, F., 2014. Deep Convection Triggering by Boundary Layer Thermals. Part II: Stochastic Triggering Parameterization for the LMDZ GCM. J. Atmospheric Sci. 71, 515–538. https://doi.org/10.1175/JAS-D-12-0337.1

Sadourny, R., Laval, K., 1984. January and July performance of the LMD general circulation model. New Perspect. Clim. Model. 173–197.

Sandu, I., Beljaars, A., Balsamo, G., Ghelli, A., 2012. Revision of the surface roughness length table. ECMWF Newsl. 8–9.

Santanello, J.A., Dirmeyer, P.A., Ferguson, C.R., Findell, K.L., Tawfik, A.B., Berg, A., Ek, M., Gentine, P., Guillod, B.P., van Heerwaarden, C., Roundy, J., Wulfmeyer, V., 2018. Land–Atmosphere Interactions: The LoCo Perspective. Bull. Am. Meteorol. Soc. 99, 1253–1272. https://doi.org/10.1175/BAMS-D-17-0001.1

Saouabe, T., Naceur, K.A., El Khalki, E.M., Hadri, A., Saidi, M.E., 2022. GPM-IMERG product: a new way to assess the climate change impact on water resources in a Moroccan semi-arid basin. J. Water Clim. Change 13, 2559–2576. https://doi.org/10.2166/wcc.2022.403

Schilling, J., Freier, K.P., Hertig, E., Scheffran, J., 2012. Climate change, vulnerability and adaptation in North Africa with focus on Morocco. Agric. Ecosyst. Environ. 156, 12–26. https://doi.org/10.1016/j.agee.2012.04.021

Schilling, J., Hertig, E., Tramblay, Y., Scheffran, J., 2020. Climate change vulnerability, water resources and social implications in North Africa. Reg. Environ. Change 20, 15. https://doi.org/10.1007/s10113-020-01597-7Su, Z., Schmugge, T., Kustas, W.P., Massman, W.J., 2001. An Evaluation of Two Models for Estimation of the Roughness Height for Heat Transfer between the Land Surface and the Atmosphere. J. Appl. Meteorol. 40, 1933–1951. https://doi.org/10.1175/1520-0450(2001)040<1933:AEOTMF>2.0.CO;2Tramblay, Y., Badi, W., Driouech, F., El Adlouni, S., Neppel, L., Servat, E., 2012. Climate change impacts on extreme precipitation in Morocco. Glob. Planet. Change 82–83, 104–114. https://doi.org/10.1016/j.gloplacha.2011.12.002

Tramblay, Y., Ruelland, D., Somot, S., Bouaicha, R., Servat, E., 2013. High-resolution Med-CORDEX regional climate model simulations for hydrological impact studies: a first evaluation of the ALADIN-Climate model in Morocco. Hydrol. Earth Syst. Sci. 17, 3721–3739. https://doi.org/10.5194/hess-17-3721-2013

Vafeidis, A.T., Abdulla, A.A., Bondeau, A., Brotons, L., Ludwig, R., Portman, M., Reimann, L., Vousdoukas, M., & Xoplaki, E. (2020). Managing future risks and building socioecological resilience in the Mediterranean. In: Climate and Environmental Change in the Mediterranean Basin – Current Situation and Risks for the Future. First Mediterranean Assessment Report [Cramer W, Guiot J, Marini K (eds.)] Union for the Mediterranean, Plan Bleu, UNEP/MAP, Marseille, France, 539-588.

Vicente-Serrano, S.M., Lopez-Moreno, J.-I., Beguería, S., Lorenzo-Lacruz, J., Sanchez-Lorenzo, A., García-Ruiz, J.M., Azorin-Molina, C., Morán-Tejeda, E., Revuelto, J., Trigo, R., Coelho, F., Espejo, F., 2014. Evidence of increasing drought severity caused by temperature rise in southern Europe. Environ. Res. Lett. 9, 044001. https://doi.org/10.1088/1748-9326/9/4/044001

Vignon, E., Hourdin, F., Genthon, C., Gallée, H., Bazile, E., Lefebvre, M.-P., Madeleine, J.-B., Van de Wiel, B.J.H., 2017. Antarctic boundary layer parametrization in a general circulation model: 1-D simulations facing summer observations at Dome C. J. Geophys. Res. Atmospheres 122, 6818–6843. https://doi.org/10.1002/2017JD026802

Vignon, E., Hourdin, F., Genthon, C., Van de Wiel, B.J.H., Gallée, H., Madeleine, J., Beaumet, J., 2018. Modeling the Dynamics of the Atmospheric Boundary Layer Over the Antarctic Plateau With a General Circulation Model. J. Adv. Model. Earth Syst. 10, 98–125. https://doi.org/10.1002/2017MS001184

Wang, F., Ducharne, A., Cheruy, F., Lo, M.-H., Grandpeix, J.-Y., 2018. Impact of a shallow groundwater table on the global water cycle in the IPSL land–atmosphere coupled model. Clim. Dyn. 50, 3505–3522. https://doi.org/10.1007/s00382-017-3820-9

Yamada, T., 1983. Simulations of nocturnal drainage flows by a q2l turbulence closure model. J. Atmospheric Sci.

Zkhiri, W., Tramblay, Y., Hanich, L., Jarlan, L., Ruelland, D., 2019. Spatiotemporal characterization of current and future droughts in the High Atlas basins (Morocco). Theor. Appl. Climatol. 135, 593–605. https://doi.org/10.1007/s00704-018-2388-6

Zobler, L. (1986). A World Soil File for Global Climate Modeling: National Aeronautics and Space Administration, Goddard Space Flight Center, Institute for Space Studies.